

1-1-2011

Synthesis of Nanotips Through Femtosecond Laser Ablation of Glass with Assisted Gas

Nikunj Patel
Ryerson University

Follow this and additional works at: <http://digitalcommons.ryerson.ca/dissertations>

 Part of the [Nanoscience and Nanotechnology Commons](#)

Recommended Citation

Patel, Nikunj, "Synthesis of Nanotips Through Femtosecond Laser Ablation of Glass with Assisted Gas" (2011). *Theses and dissertations*. Paper 1473.

**SYNTHESIS OF NANOTIPS THROUGH FEMTOSECOND
LASER ABLATION OF GLASS WITH ASSISTED GAS**

by

Nikunj Patel

Bachelor of Engineering

Ryerson University, 2009

A Thesis

presented to Ryerson University

in partial fulfillment of the
requirements for the degree of
Master of Applied Science
in the Program of
Aerospace Engineering

Toronto, Ontario, Canada, 2011

© Nikunj Patel, 2011

AUTHOR'S DECLARATION

I hereby declare that I am the sole author of this thesis.

I authorize Ryerson University to lend this thesis to other institutions or individuals for the purpose of scholarly research.

Nikunj Patel

Ryerson University

I further authorize Ryerson University to reproduce this thesis by photocopying or by other means, in total or in part, at the request of other institution or individuals for the purpose of scholarly research.

Nikunj Patel

Ryerson University

ABSTRACT

SYNTHESIS OF NANOTIPS THROUGH FEMTOSECOND LASER ABLATION OF GLASS WITH ASSISTED GAS

Nikunj Patel, Master of Applied Science, 2011

Department of Aerospace Engineering, Ryerson University

Nanotips are the key nanostructures for many applications. Until now, the nanotips of only the crystalline materials have been produced via various deposition methods which require sophisticated equipment, high vacuum, and clean room operations. This thesis proposes a single step, rapid synthesis method using femtosecond laser irradiation at megahertz frequency with background flow of nitrogen gas at ambient conditions. Amorphous nanotips are obtained without the use of catalyst. The nanotips grow from highly energetic plasma generated when target is irradiated with laser pulses. The vapor condensates, nanoparticles and droplets from the plasma get deposited back on to the hot target surface where they experience force imbalance due to which the stems for the nanotips growth are initiated. Once the stems are generated, the continuous deposition of vapor condensates provides building materials to the stems to complete the growth of nanotips. Further study found that the growth of the nanotips is influenced by laser parameters and gas conditions.

ACKNOWLEDGEMENTS

I would like to take this moment to express my sincere appreciation for my supervisors Dr. Bo Tan and Dr. Krishnan Venkatakrishnan for their invaluable guidance, encouragement, and inspiration throughout the research work for the graduate study. Without their support, the completion of this thesis would not have been possible.

I would also like to thank all the technical lab support staff at Ryerson University who directly or indirectly helped me throughout my research work.

I would like to extend my gratitude towards my friends and family for their unconditional love, support, and encouragement for my success in graduate study. Finally, I would like to acknowledge my long time academic peers and close friends (*Palneet and Krunal*) for making my school life full of fun and their motivation at tenacious times.

DEDICATION

I would like to dedicate this work to my parents for their endless love:

to mom, Dipti, for supporting me every step of the way,

to dad, Bharat, for being encouraging and inspiring.

I would also like to dedicate this work to my beloved wife, *Falguni*, for her support, inspiration and patience to see me succeed at the level of graduate study.

Extended dedication to my Family for being part of my life and making it wonderful:

Bharat, Dipti, Hitendra, Kalapna, Ishwarbhai, Laxmiben,

Pooja, Mehul, Dhruti,

Shivani, Shiv.

Further dedication to my close friends: *Vivek, Chirag and their parents (Dipak-uncle and Mala-aunty) and Sweta*

TABLE OF CONTENTS

AUTHOR'S DECLARATION	II
ABSTRACT.....	III
ACKNOWLEDGEMENTS	IV
DEDICATION.....	V
LIST OF FIGURES	VIII
LIST OF APPENDICES	X
NOMENCLATURE.....	XI
CHAPTER 1: INTRODUCTION AND OVERVIEW.....	1
1.1 EXISTING NANOTIPS FABRICATION METHODS	2
1.1.1 <i>Chemical Vapour Deposition Technique (Vapor-Solid Growth)</i>	2
1.1.2 <i>Electron cyclotron resonance (ECR) plasma etching</i>	5
1.1.3 <i>Modified Thermal Evaporation Process</i>	6
1.1.4 <i>Summary</i>	7
1.2 LASER AND DIELECTRIC MATERIAL INTERACTIONS	8
1.3 FEMTOSECOND LASER SYNTHESIS OF NANOTIPS FROM DIELECTRIC TARGETS	10
1.4 RESEARCH OBJECTIVES	12
CHAPTER 2: PLASMA-PLUME EXPANSION DYNAMICS.....	13
2.1 PLASMA EXPANSION INSIDE A CHAMBER UNDER VARIOUS GAS PRESSURES	13
2.2 PLASMA EXPANSION IN OPEN AIR UNDER AMBIENT CONDITION AT ATMOSPHERIC PRESSURE.....	18
2.3 SUMMARY	22
CHAPTER 3: EXPERIMENTAL SETUP	24
CHAPTER 4: PROPOSED GROWTH MECHANISM	27
4.1 BACKGROUND KNOWLEDGE.....	27
4.2 NANOTIP GROWTH MECHANISM.....	28
4.3 SUMMARY	35

CHAPTER 5: INFLUENCE OF FEMTOSECOND LASER PARAMETERS ON GROWTH OF NANOTIPS.....	37
5.1 EFFECT OF PULSE WIDTH.....	37
5.2 EFFECT OF LASER PULSE REPETITION RATE	43
5.3 EFFECT OF DWELL TIME	47
5.4 EFFECT OF LASER POLARIZATION	52
CHAPTER 6: CONCLUSION AND FUTURE WORK.....	56
6.1 CONCLUSION.....	56
6.2 FUTURE WORK PROPOSAL	57
APPENDIX.....	59
REFERENCES.....	70

LIST OF FIGURES

Figure 1-1: SEM images of quasi-aligned AlN nanocones grown on a Ni-coated silicon wafer under 700C.....	3
Figure 1-2: Schematic representation of the nanotips formation.....	5
Figure 1-3: Schematic representation of the modified thermal-evaporation system used for the generation of ZnO nanonails.....	6
Figure 1-4: SEM images of nanofibrous structure and platelet-shaped nanotips on femtosecond laser-irradiated glass. (a) without background gas, and (b) with nitrogen background gas flow .	10
Figure 2-1: Temporal sequences of the plume self-emission at different background gas pressure	15
Figure 2-2: Resonance-absorption shadowgraphs showing the morphology for single-pulse ablation plumes on an aluminum target for various pulse durations	18
Figure 2-3: Resonance-absorption shadowgraphs of the material-vapor distribution and shock waves of plume generated by high repetition rate drilling of aluminum target.....	19
Figure 2-4: Schematic of a surrounding gas mixing into plasma jet generated commercial plasma torch	21
Figure 3-1: Schematic representation of the experimental setup.....	24
Figure 3-2: Arrangement of nitrogen gas tubes and specimen	25
Figure 4-1: a) SEM image of femtosecond laser irradiated glass surface, b) corresponding EDX results	29
Figure 4-2: Comparison for XRD results of femtosecond laser a) non irradiated glass with no nanotips, b) irradiated glass specimen covered with nanotips.....	29
Figure 4-3: a) Schematic of the forces experienced by deposited droplets, b) SEM images of droplets with tips` stems (laser parameters: 214fs, 13MHz, 0.75ms dwell time).....	31

Figure 4-4: a) Types of tips formed after laser irradiation of soda-lime glass surface A) Flower like formation, b) Tips growth from deposited film of molten glass film, and c) Individual tip growth	32
Figure 4-5: Schematic for growth steps of nanotips	33
Figure 5-1: Micro holes drilled by femtosecond pulses with pulse width a) 214fs and b) 714fs.	39
Figure 5-2: Tips generated at 214fs for 13MHz at dwell time of 0.5ms	41
Figure 5-3: SEM images of nanotips grown in target irradiated with a) 214fs, b) 428fs and c) 714fs laser pulses	42
Figure 5-4: Nanotips generated for the average laser power of 16W for pulse repetition rates of a) 4MHz, b) 8MHz, and c) 13MHz; the dwell time was 0.5 ms for all three cases.....	45
Figure 5-5: Nanotips growth stages at 8MHz repetition rate for dwell times of (a) 0.1ms, (b) 0.25ms, and (c) 0.50ms	48
Figure 5-6: Nanostructures generated at dwell time of 0.75ms for the repetition rate of (a) 4MHz, (b) 8MHz, and (c) 13MHz	49
Figure 5-7: Growth stages of plasma expansion and nanotips formation.....	51
Figure 5-8: SEM images of glass targets irradiated with circularly polarized pulses (a,b,c), and linearly (p-) polarized laser pulses (d,e,f): a),d) 4MHz, 0.25ms; b),e) 4MHz, 0.5ms; c),f) 8MHz, 0.25ms.....	54

LIST OF APPENDICES

Appendix A: Nanotips generated for circular polarization.....	59
Appendix B: Nanotips generated for linear polarization	62
Appendix C: Nanotips generated on window glass	67
Appendix D: List of Journal Submissions	69

NOMENCLATURE

1D	1 Dimensional
MHz	Megahertz (10^6 Hz)
kHz	Kilohertz (10^3 Hz)
ns	Nanosecond (10^{-9} s)
ps	Picosecond (10^{-12} s)
fs	Femtosecond (10^{-15} s)
μ s	Microsecond (10^{-6} s)
ms	Millisecond (10^{-3} s)
nm	Nanometer (10^{-9} m)
μ m	Micrometer (10^{-6} m)
cm	Centimeter (10^{-3} m)
in	Inches
W	Watt (J/s)
eV	Electron Volt
$^{\circ}$ C	Degree Celsius
J	Joule
μ J	Micro-Joule (10^{-6} J)
UV	Ultra violet
t	Time
z	Axial location in laser focal region ($z= 0$ at focal point)
τ_p	Laser pulse duration (width)

c	Speed of light in the medium
β	Ratio of peak pulse power to the breakdown threshold of a material (P_{\max}/P_{th}),
P_{\max}	Average maximum laser power
P_{th}	Breakdown threshold laser power of a material
Z_R	Rayleigh range or focal region
λ	Wavelength of the laser beam
n	Refractive index of the medium
w_0	Laser beam radius at the focal point
z	Axial position in focal region

Chapter 1: Introduction and Overview

Nanoscale technologies have experienced tremendous growth in past several years. Majority of this growth is attributed to the discovery of new nanostructured materials exhibiting enhanced properties that can be used in practical applications. Due to their distinctive optical, electronic, mechanical, chemical and other properties, a series of oriented 1D structure such as nanocones, nanotubes, nanotips, nanowires, and nanofibers have become of enormous interest to today's scientific research community [1]. Out of all these 1D nanostructures, the nanotips of different materials are attractive and stimulating due to their lower symmetry than the wires, tubes, rods, and belts; and thus they have always puzzled the scientists for their self-assembly of such morphology in a synthetic process [2]. The unique properties of these 1D nanostructures have made themselves useful in applications of nano-featured technologies, such as field-emission displays, laser diodes, scanning probe microscopy, solar cells, and biosensors [1, 2].

Nanotips/Nanocones of different materials (carbon, silicon, poly silicon, GaN, GaP, sapphire, Al, AlN, ZnO, and ZnCdSeTe) have been produced using techniques such as self-masking dry etching technique in an electron cyclotron resonance (ECR) plasma process, vapor-liquid-solid (VLS) mechanism, thermal evaporation technique, chemical vapor deposition (CVD), plasma-enhanced hot filament CVD, Physical Vapor deposition [2-7]. However, the femtosecond laser-induced breakdown is attracting major interest of research for many investigators around the world for number of reasons. The main advantage of using femtosecond laser pulses is that it does not require a clean room environment, offers high speed machining and induces lower residual thermal effects compare to other techniques [8]. However before jumping into growth

mechanism of nanotips induced by femtosecond laser pulse irradiation, it is important to understand the existing nanotips fabrication methods to realize the benefits of currently proposed femtosecond laser generated nanotips growth.

1.1 Existing Nanotips Fabrication Methods

The nanotips of various materials have been produced using many different techniques. Some of these techniques are various forms of Chemical Vapor deposition (CVD), physical vapor deposition, etching techniques, electron beam-induced deposition, and thermal vapor deposition.

1.1.1 Chemical Vapour Deposition Technique (Vapor-Solid Growth)

The Chemical Vapor Deposition (CVD) is one of the widely utilized techniques for the growth of many different nanostructures. It is used in many different forms such as radio-frequency plasma enhanced CVD (RF-PECVD), hot-filament CVD (HF-CVD), thermal CVD (T-CVD), metal organic CVD (MO-CVD), microwave plasma enhanced CVD (MW-PECVD), and electron cyclotron resonance plasma enhanced CVD (ECR-PECVD). In a typical CVD technique, the precursor gases are delivered into the reaction chamber using carrier gasses at around ambient temperatures. A heated substrate is placed inside reaction chamber. The precursors react/decompose to form desired solid products as they pass over or come into contact with a heated substrate. The desired solid products get deposited onto substrate and the by-products are removed by carrier gas via outlet.

Chun Liu, et al. grew Aluminum Nitride nanocones using a typical CVD on a catalyst (Ni) coated n-type Si(111) wafer [6]. The precursors used as aluminum and nitrogen sources were AlCl_3 and NH_3/N_2 (NH_3 , 4 vol %). The coated silicon wafer substrate was placed in the center of an alumina tube inside a horizontal tubular furnace. At first the system is evacuated and flushed with Ar several times to remove oxygen and moisture, and then the temperature of the furnace was elevated to 700°C . Subsequently, the AlCl_3 was vaporized in the front of alumina tube at 140°C and carried to the reaction zone by Ar flow, where it reacted with NH_3/N_2 flow. The product, AlN, of the precursors gets deposited on the Ni-coated Si wafer for the operation duration of 4h to form nanocones. Once the whole operation is completed, the system is cooled to ambient temperature by Ar flow.

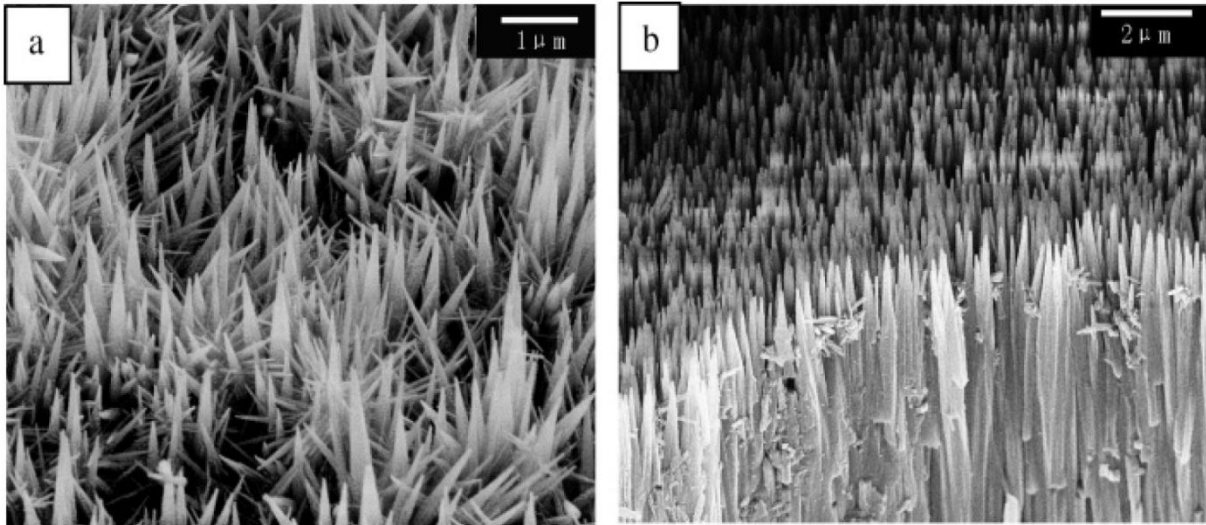


Figure 1-1: SEM images of quasi-aligned AlN nanocones grown on a Ni-coated silicon wafer under 700°C : (a) tilted view, (b) side view [6]

The film of Ni on Si wafer acts as catalyser for the reaction between AlCl_3 and NH_3 to form the nanoparticles of AlN. The nanoparticles get deposited onto the substrate surface to form a thin film until it reaches a certain critical thickness. Once the critical thickness is reached, the AlN

nanocrystals started forming because of the inherent strain induced by the lattice mismatch between the AlN and Ni films. Figure 1-1 shows the SEM images of the quasi-aligned AlN nanocones grown on Ni-coated Si wafer. As can be seen the nanocones grew perpendicularly oriented to the wafer surface to form the quasi arrays. This perpendicular growth is due to the inherent asymmetry of the hexagonal crystal structure along the c-axis of AlN. This promoted the subsequent preferential growth of one-dimensional nanostructures along the [001] direction. The catalyst (Ni) is fixed to the Si wafer surface during the growth process to catalyze the reaction of precursors to continuously produce the AlN species. As a result it is logical to consider that the growth of nanostructures along the [001] direction as there is a progressive decrease in the amount of the AlN species produced resulting in the formation of nanocones. Similarly, the nanotips of other material have also been produced using different form of CVD.

ZnO is attracting the major interest for the applications in nanoscale electronic and photonic devices due its properties such as being a direct wide band gap (3.32eV) semiconductor with high exciton-binding energy of 60 meV. As a result, the nanotips made from ZnO are very important and have been grown by many different researchers using various techniques. J. Zhong generated ZnO nanotips using metal-organic CVD on n-type Si wafer and silicon-on-sapphire (SOS) substrates in a vertical flow MOCVD system at low pressure [9, 10]. The MOCVD is the technique more preferable than typical CVD and many other techniques such as vapor-phase transport, catalyst assisted molecular-beam epitaxy because it is performed at low pressure and temperature. The MOCVD does not require the pre-deposition of a metal catalyst onto the substrate surface for the growth of ZnO nanotips. The diethylzinc was used as the Zn metal-organic source while oxygen and triethylgallium were used as oxidizer, and Ga-doping

source, respectively. The ZnO nanotips grew in temperature range between 400 and 500 °C. The nanotips grew on Si substrate were very dense and mainly oriented along c-axis with bottom diameter ranging from 40-60 nm and the length ~ 500nm.

1.1.2 Electron cyclotron resonance (ECR) plasma etching

One of the very efficient techniques for the nanofabrication is the dry etching of the substrates pre-treated with heterogeneous nanomasks. ECR plasma etching is the one-step, self-masked dry etching technique which has been utilized by many researchers to generate nanotips of various materials. For example, Chih-Hsun Hsu, et al. produced nanotips with nanoscale apices (~1 nm) with high aspect ratios (~ 50) [11]. They used Seki high-density electron cyclotron resonance (ECR) plasma reactor. The schematic of growth process is depicted in Figure 1-2.

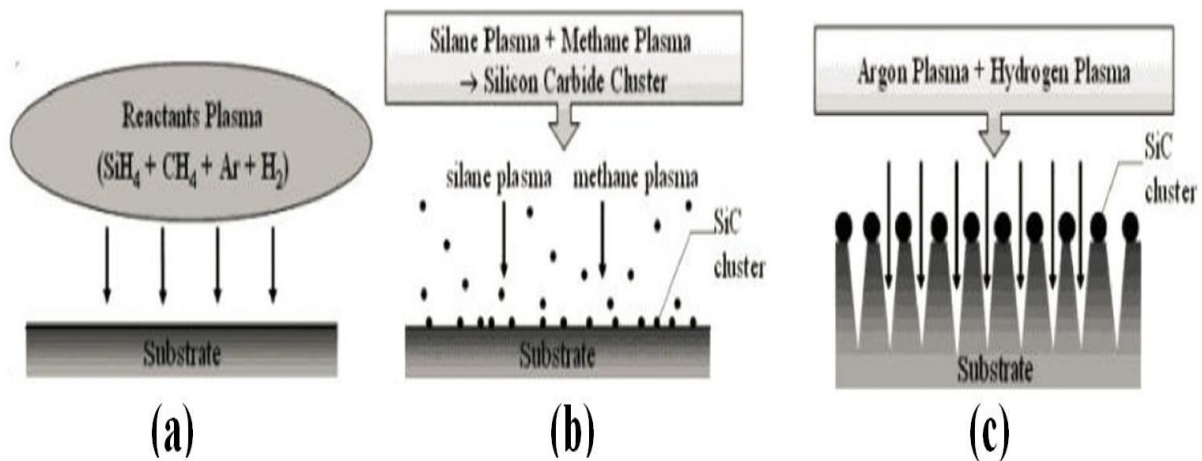


Figure 1-2: Schematic representation of the nanotips formation: (a) reactive gases are composed of silane, methane, argon, and hydrogen; (b) the SiC nanosized clusters are formed from the reaction of SiH_4 and CH_4 plasma and uniformly distributed on the substrate surface; and (c) the unmasked region is etched by Ar and H_2 plasma, whereas the region masked by SiC caps protects the substrate from etching, and hence creates the conical tips [11]

The substrate is cleaned by hydrogen (H_2) plasma prior to the simultaneous masking and etching process in the reaction chamber under vacuum. Subsequently, the precursor gases containing (SiH_4 & CH_4 plasma) to form nanosized clusters of SiC to form uniformly distributed nanomasks over the substrate surface and simultaneously the plasma of Ar and H_2 gas is introduced to perform physical and chemical etching respectively of unmasked substrate surface to develop nanotips. Due to their hardness and chemical inertness against etching gases, SiC nanoclusters act as protective caps to form high density and high aspect ratio nanotips arrays as depicted in Figure 1-2c.

1.1.3 Modified Thermal Evaporation Process

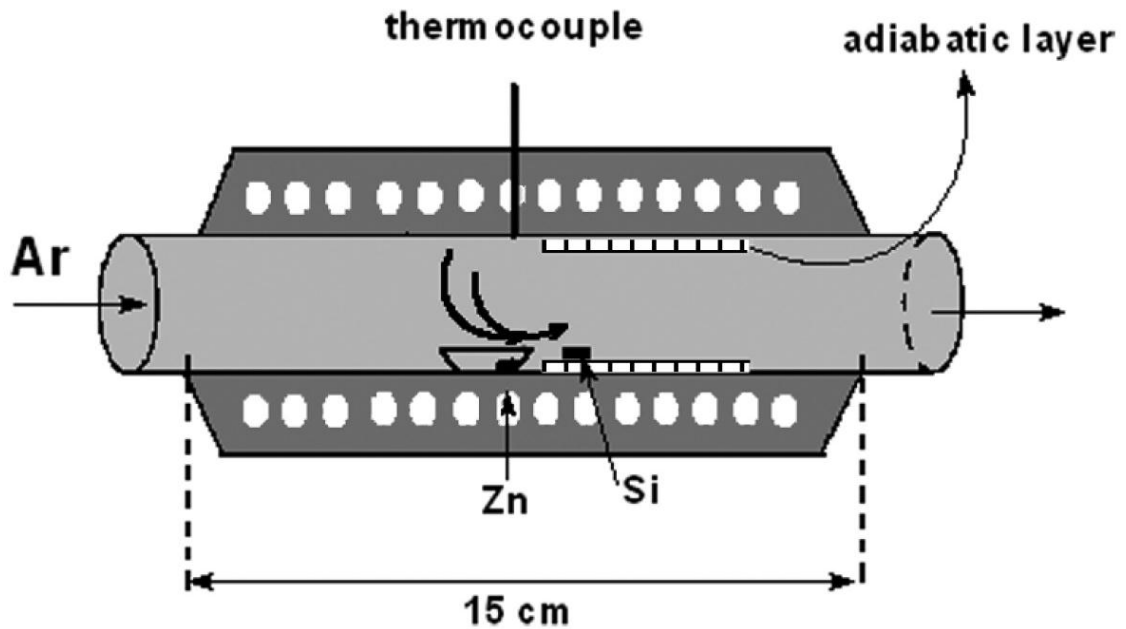


Figure 1-3: Schematic representation of the modified thermal-evaporation system used for the generation of ZnO nanonails [12]

Figure 1-3 schematic of the system used to grow ZnO nanonails on a Si substrate using modified thermal-evaporation process [12]. This system was made of quartz tube furnace in which

adiabatic layers were used for special purpose as depicted in Figure 1-3. The p-type (100)-oriented silicon was used as the substrate to collect the ZnO nanostructures. This silicon substrate was placed on an adiabatic layer to make sure an abrupt temperature decrease and the high gas concentration for the growth of vertically aligned ZnO nanonails. The Zinc powder was used as the Zn source which was placed in an alumina boat placed in proximity of adiabatic layer near where the silicon substrate was placed as shown in Figure 1-3. The Ar gas was used as carrier. Prior to growth process begin; the quartz tube was flush out with high-purity Ar gas for 10 minutes. Then furnace was heated to 600°C to promote the growth of vertically aligned ZnO nanonails. The vertical distance between the source material and the substrate was 10-20 mm so that evaporated Zn atoms could easily land on the silicon substrate. The reaction was lasted for 60 minutes in presence of Ar gas flow with the flow rate of 500 SCCM (standard cubic centimetres per minutes). Then the furnace was cooled down to room temperature. The ZnO nanonails grew as gray-white product of chemical reaction of Zn on the substrate surface.

1.1.4 Summary

In summary, various methods for the growth of nanotips utilized in past and in current time have been discussed. As can be seen from above descriptions that in techniques such as modified thermal evaporation, chemical vapor deposition (CVD) and ECR plasma etching, the process has to be done in a close chamber that has to be heated up to high temperatures for growth of the nanotips to occur. Also, the building material of the nanotips in most of the above processes, for example for ZnO nanotips using CVDs, has to be brought to the substrate surface by carrier gas. In the case of thermal evaporation, the building material of the nanotips is in solid form and placed in a container inside the reaction chamber. This container is heated to high temperatures

so that the building material is evaporated and brought to the substrate sample by carrier gas where further reactions occur and the final products get deposited to the substrate sample. In CVD process, the building materials are in form of precursors chemical which are brought into the reaction chamber by carrier gas. The reaction chamber has to be vacuumed and heated up so that the precursors chemicals can breakdown and react to each other to form desired products that get deposited on to the substrate sample. In most of the cases in CVD process, the substrate surface has to be coated with a film of catalyst layer to promote the reaction. In ECR plasma etching, the substrate is placed in a chamber and bombarded with plasma species consisting of mixtures of various chemical compounds. Some products of reaction in plasma get deposited on to the substrate surface to act as mask against the etching caused by rest of the plasma species. In conclusion, all the aforementioned techniques require very sophisticated equipment to produce ideal environment for the nanotips to grow and the operation requires multiple number of intermediate steps and long processing time.

1.2 Laser and Dielectric material interactions

The residual thermal effects are greatly reduced in target material when it is ablated with laser pulses in subpicosecond and femtosecond time scale compared to the pulses with nanosecond-long Q-switched laser pulses [8]. The main reason for this is that the time for conduction of energy from the laser interaction site by thermal diffusion is very short. Femtosecond laser breakdown threshold fluence does not follow the usual scaling of $\tau^{1/2}$ which is valid for the long-pulsed laser ablation [8, 13]. The breakdown mechanism is quite different for ultra-short laser pulses compared to long-laser pulses. Stuart B. C., et al performed an extensive study of laser-induced damage threshold measurements on dielectric materials (fused silica and alkali

fluorides) for pulse durations τ ranging from 140fs to 1ns. They discovered the decreasing threshold fluence with a gradual transition from the long-pulse, thermally dominated regime to an ablative regime dominated by collisional and multiphoton ionization, and plasma formation [13]. Wide-band-gap dielectric materials are normally transparent to visible and near-infrared light as the photon energy is insufficient to excite an electron from the valence to the conduction band by linear absorption. As a result the breakdown of the target starts with the excitation of valence-band electrons by the incident laser pulses. An electron in the valence band can absorb several visible or near-infrared photons and gain enough energy to cross the band gap [14]. This process is referred to as multiphoton ionization. In femtosecond range, the breakdown intensities are so high that the multiphoton ionization alone is strong enough to produce electron densities high enough to cause damage. The interaction of the ultrashort pulses with the target is so short that energy is absorbed by the electrons much faster than it is transferred to the lattice [13]. This nonlinear photoionization create free electrons which absorb more energy from the laser pulse by inverse bremsstrahlung [14]. As a result, only some part of the energy delivered by first few femtosecond pulses is absorbed via conductive electrons on the surface [8, 13]. Rest of the energy gets transmitted and refracted elsewhere. These free electrons absorb laser energy until certain threshold value; during which energy gets dissipated to adjacent lattice and gets accumulated as more laser pulses are delivered to the surface of the target. The accumulated energy creates colour centers, irregularities, micro cracks on the dielectric surface which increases the absorptivity of the irradiated surface [13, 15]. As a result, for subsequent laser pulses, great portion of energy is absorbed. When the accumulated energy passes the conductive threshold energy barrier for the electrons, it expulses the electron, neutrals, and ions from the surface which makes the fast component of the expanding plume. The release of the electrons

breaks down the chemical bonds between the atoms in the top few lattice [8]. Due to the breakdown of the bonds, the lattice becomes loose, melts down and creates a pool of molten material as more energy is absorbed. The subsequent laser pulses along with shock waves eject the nanoparticles and fluid drops from the molten pool forming the slow component of plasma plume which expands outward over the laser focus spot and covers the target surface.

1.3 Femtosecond laser synthesis of nanotips from dielectric targets

Previous research by the research group of Laser Micro Nano Manufacturing Lab at Ryerson University showed that femtosecond laser is capable of generating nanotips [1]. When glass target was irradiated with femtosecond laser without assist gas, the fibrous networks of agglomerated nanoparticles were formed. With nitrogen gas flow, nanotips were obtained which were much larger in size than the fibrous networks. However, the process was unrepeatable and uncontrolled due to the lack of clear understanding of the formation mechanism.

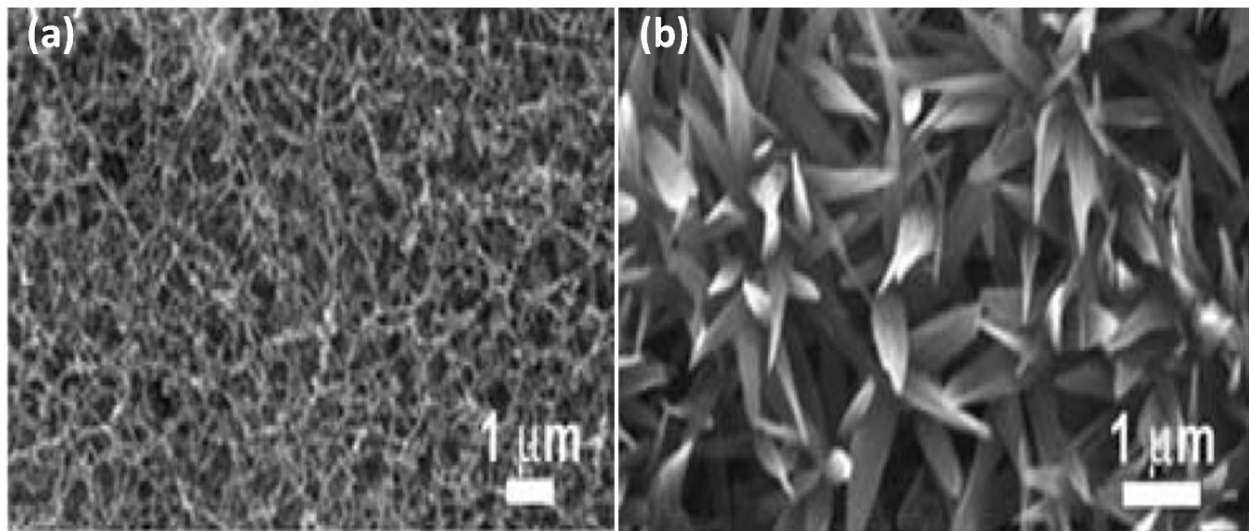


Figure 1-4: SEM images of nanofibrous structure and platelet-shaped nanotips on femtosecond laser-irradiated glass. (a) without background gas, and (b) with nitrogen background gas flow [1]

Figure 1-4 shows the SEM images of the nanostructures generated on the femtosecond laser irradiated glass containing 53 mol% SiO₂, 23 mol% Na₂O, 20 mol% CaO and 4 mol % P₂O₅. When the glass was irradiated without background gas flow in ambient air, the weblike nanofibrous structure was formed on the glass surface as seen in Figure 1-4a. It has been suggested that this nanostructure are generated due to agglomeration of glass nanoparticles. The nanoparticles are generated from the plasma due to vapor condensation. The cooling time of these nanoparticles is much larger than pulse separation time. As a result, the nanoparticles generated from successive laser pulse are fused to the particles created from the previous laser pulse that are still above the melting temperature and grow nanofibrous structures. However, when the irradiation is done in the background of nitrogen gas flow, the nanoscale tips are formed surrounding the laser-irradiated spots on glass target as depicted in Figure 1-4b. Due to the collisions between the nitrogen gas molecules and plasma, the pulse expansion is slow down and thus the vapor condensation is greatly delayed. This delay results in coalescence of the several nuclei formed during condensation which further results in formation of larger nanoparticles. These larger nanoparticles then get assembled into nanotips formations which are much larger in size compare to nanofibrous networks. The previous research was just limited to explain the reason why there were size difference between nanostructures generated with and without background nitrogen gas. However, the actual explanation to how the nanotips are formed in random directions and why their cross sectional area reduces along their length was not explored.

1.4 Research Objectives

This research was developed based on the earlier research finding from femtosecond laser ablative synthesis of nanotips. Thus, the main objective of this research is to understand the growth mechanism of the leaf-like nanotips produced on femtosecond laser irradiated dielectric target which was only possible in the presence of the background nitrogen gas flow.

In addition, this research also attempt to understand how the growth is influenced under various laser conditions such as different laser pulse durations (widths), pulse repetition rates (also known as laser pulse frequency), laser dwell times, and various laser beam polarization. Studying the nature of nanotips growth under aforementioned laser conditions would give us better understanding to produce more controlled and uniform growth of nanotips over the target surface.

Chapter 2: Plasma-Plume Expansion Dynamics

The highly energetic plasma is becoming part of many practical applications such as plasma vapor deposition, pulsed laser deposition for thin-film depositing, plasma welding and commercial plasma spray torch. In all of the aforementioned applications, the final products of the process are greatly affected by how the utilized plasma expands and interacts with surrounding environment. The synthesis technique for the nanotips that has been proposed in this thesis is also dependent on the plasma generated from irradiation of target material using femtosecond laser. As a result, it was important to understand the nature of plasma expansion. In this chapter, the influence of various conditions on the plasma expansion has been discussed.

2.1 Plasma expansion inside a chamber under various gas pressures

Femtosecond laser ablation of metals and semiconductors in vacuum has been investigated broadly due to its application in generation and deposition of nanoparticles for thin films production. From these studies it was discovered that the plume is comprised of two main components: (a) a first part is made of fast atomic species (electrons, ions and neutrals), which leaves the target surface with high expansion velocities (\sim few tens of km/s) and (b) a second component is much slower mainly comprised of nanoparticles and droplets of the target material which expand with velocities much smaller than the atomic plume [16, 17]. The fast component originate from the topmost surface lattices of the target material which directly decomposed into a vapor phase leading to the generation of an atomic components, whereas the slow component of the plasma is generated as an end result of the decomposition of the material located more

deeply into the original solid target due to melting, phase explosion and mechanical fragmentation. Recently, Amoruso et al. conducted an experimental analysis on the propagation of iron (Fe) plume generated using femtosecond laser (wavelength= 527nm, pulse width ~300fs) ablation in background air for a range of pressure from high vacuum up to tens of millibars [16]. The findings of their experimental analysis are summarized in Figure 2.1 showing the temporal sequences of the plume expansion at different air pressures. They found that the atomic plume (the fast component) expansion behaviour experience a transformation from a forward-directed propagation at low pressure to a spherical-like expansion at high pressure, being stopped at distance of less than 1 cm from the target surface at around a pressure of few millibars. However, the nanoparticles plume (slow component) maintains a forward-directed expansion and is much less confined by the ambient gas reaching a plume stopping regime only for a pressure of tens of millibars.

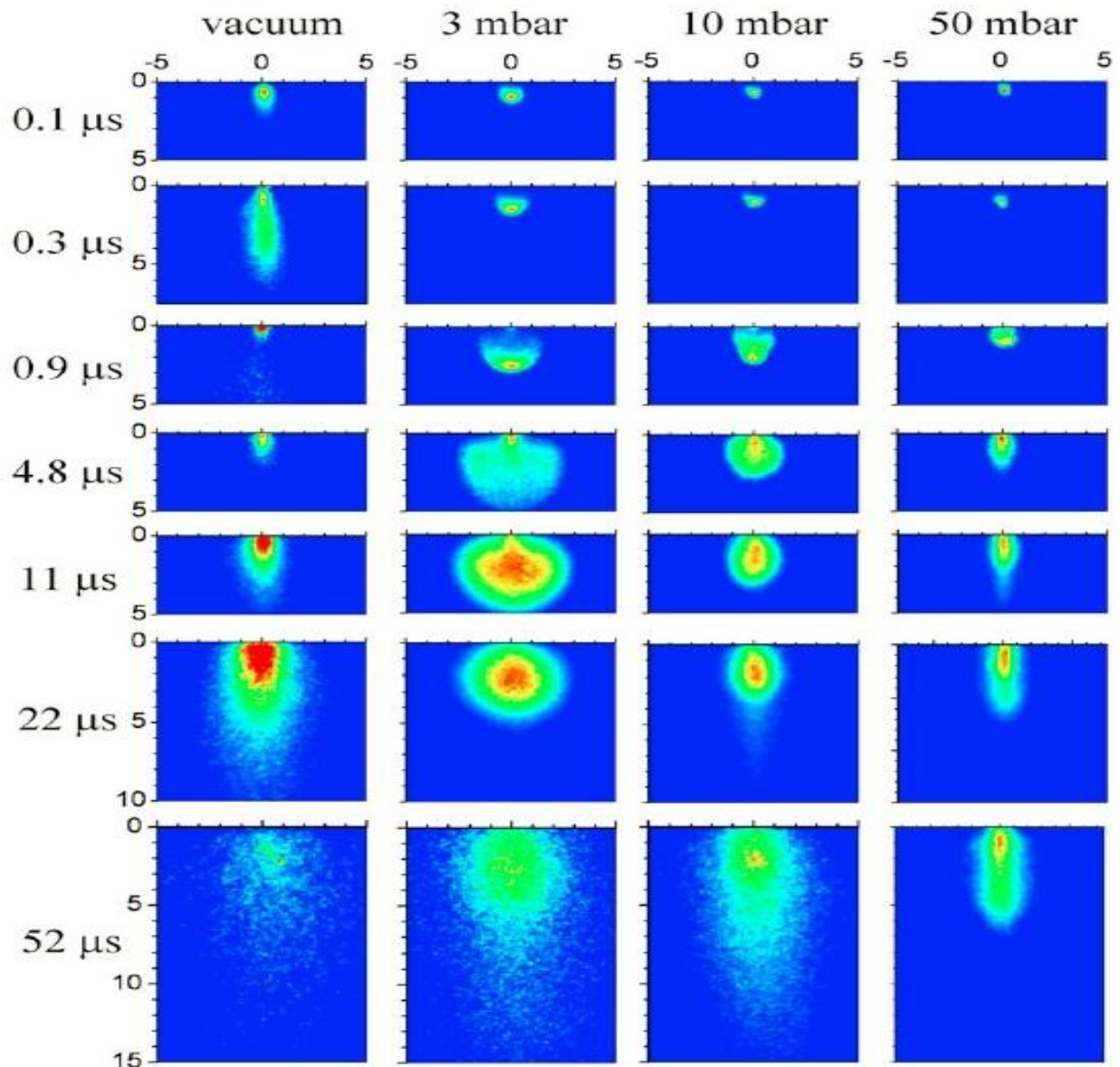


Figure 2-1: Temporal sequences of the plume self-emission at different background gas pressure. The time on the left side of the snapshots corresponds to the time delay after the laser pulse. The axes of the images report a scale in millimetres. Each ICCD image is obtained from a different laser shot and is normalized to its own maximum intensity [16]

In vacuum condition, the fast atomic plume component experiences mainly the forward-peaked expansion traveling to distances of several millimetres from the target surface in a timescale as short as hundreds of nanosecond as seen in first column of Figure 2-1. On the other hand, the slow plume component under vacuum conditions remains confined very close to the target

surface for the longer time and its full dynamic expansion only occurs after several μs . Further analysis of their experiment showed that the fast and slow plume components expand almost freely with a front velocity of $(1.6\pm 0.1) \times 10^4$ and $(5.2\pm 0.2) \times 10^2$ m/s, respectively at low pressure. As the delay time after laser pulse progresses the velocity of the slow plume component gradually reduces and the expansion behaviour broadens to become more and more hemispherical. At a much longer time delay ($\sim 20\mu\text{s}$), fast plume expansion continues to slow down and reaches a stationary behaviour and the slow component overtakes the stationary atomic plume and propagates longer distances in forward direction. As the air pressure is increased, the atomic (fast) plume component remains more and more confined to the target surface and stop traveling at a distance no further than $\sim 3\text{mm}$ after a few μs . Whereas the slow component as observe in Figure 2-1 columns for air pressure 10mbar and above starts extending longer distances than the stationary atomic plume at $10\mu\text{s}$ delay time. As the air pressure is further increased, the slow component mainly travels along the normal direction to the target surface and become spatially broader only at longer time delays. The slow component is mainly in forward direction irrespective of the gas pressure as a consequence of the high mass ratio between the nanoparticles and the ambient gas molecules.

Another research group studied the formation of nanoparticles in a plasma generated by the interaction of ultra-short laser pulses (laser pulse width 100fs, laser wavelength 800nm) with gold (0.5mm with $10 \times 10 \text{ mm}^2$ area) under various conditions such as different laser fluences ($0.4\text{J}/\text{cm}^2$ and $2.2\text{J}/\text{cm}^2$) and different interacting number of laser pulses [17]. Their experiments were performed in stainless-steel vacuum chamber with a residual pressure of 10^{-4} Pa. It is also observed as in [16] that plasma has two components (fast and slow) that expand outward at

different speed. The fast component was traveling at velocity of about 2×10^3 m/s and mainly comprised of neutral atoms and single-charged ions. On the other hand the slow part of the plasma was consisting of nanoparticles propagating at velocity about two times smaller in magnitude than that of the fast component. Furthermore when the experiments were repeated with different combinations of laser pulses and fluence (4500 laser pulses with $0.4\text{J}/\text{cm}^2$; 500 laser pulses with $2.2\text{J}/\text{cm}^2$), it was found that average nanoparticles size increased with the increasing magnitude of laser fluence.

Geohegan et al. performed a photoluminescence and Rayleigh-scattering analysis of the plasma expansion dynamics produced by pulsed laser ablation of c-Si into 1-10 Torr He and Ar gases using in turbopumped vacuum chamber [18]. They discovered that the mass ratio between plume (Si) species and background gas atoms (Ar or He) induced a major effect on the plume dynamics in the 0-1 Torr pressure rang. What it means is that the heavier Ar atoms (atomic mass = 40) can efficiently prevent Si atoms (atomic mass = 28) from the forward-going motion and even back scatter them toward oncoming plasma even at a low pressure of 1.0 Torr. This will result in a stationary, uniformly distributed nanoparticles cloud at little longer time. On the other hand when the plasma is expanding in lighter weight He gas (atomic weight = 4), the gas molecules just gradually slow down the silicon plume and angularly segregating most of the nanoparticles to a turbulent smoke ring even at a vacuum pressure as high as 10 Torr. The turbulent behaviour results in the well mixing of plasma species and surrounding gas molecules. Similar results were also found by other research group who conducted the expansion of aerosols generated by irradiating brass target by nanosecond and femtosecond laser pulses at atmospheric pressures in background of argon and helium gas [19].

2.2 Plasma expansion in open air under ambient condition at atmospheric pressure

The plasma expansion inside a chamber is more confined and uniform due to a constant pressure of gas inside a chamber as discussed in above section. However when the plasma is generated in open ambient air, a completely different dynamics occur. When the ultra-short pulsed laser beam is focused under ambient atmosphere, the high intensities of the laser pulse create a gas breakdown which creates the gas-dynamic shock wave front almost entirely in front of the nominal focal plane [20]. Breitling et al. captured resonance-absorption shadowgraphs of a laser-induced ablation plume generated from an aluminum target with various laser parameters. Figure 2-2 shows the shadowgraph of the plume generated by a single pulse for various pulse durations. As can be seen from the figure, the plume of actual ablated aluminum vapor (dark region) is enclosed inside the hemispherical shock waves (bubble like structure around the dark region) in air. Also a second shock wave front is found to be expanding along the beam axis of the laser irradiation due to the gas breakdown, which initiated due to the high intensities of ultra-short laser pulses in the focal region.

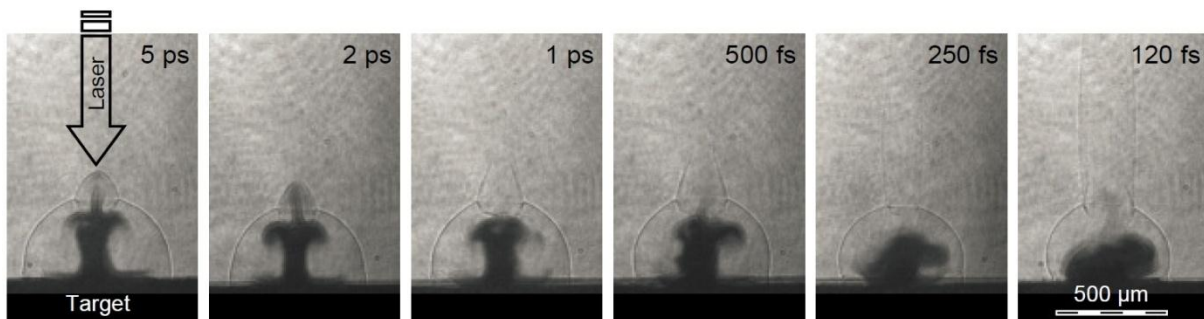


Figure 2-2: Resonance-absorption shadowgraphs showing the morphology for single-pulse ablation plumes on an aluminum target for various pulse durations. Laser parameters: wavelength (λ) = 800nm and pulse energy $Q = 500\mu\text{J}$ [20]

As can be seen from Figure 2-2, there are two shock wave fronts, the main one demonstrate spherical symmetry enclosing the aluminum vapor plume and expands radially outward from the ablation zone. The second shock is caused by gas breakdown from laser pulses interaction and shows the cylindrical symmetry along the beam axis of incoming laser pulses. As the pulsewidth of the laser is reduced close to hundred femtoseconds, the second shock wave become more and more pronounced due to stronger laser radiation-atmosphere interactions as can be seen from last image of Figure 2-2. The aluminum vapor plume inside these shock waves also experiences a transformation from being more regular mushroom-could expansion to rather turbulent behaviour as the pulse duration is reduced from few picosecond to as short as hundred femtosecond.

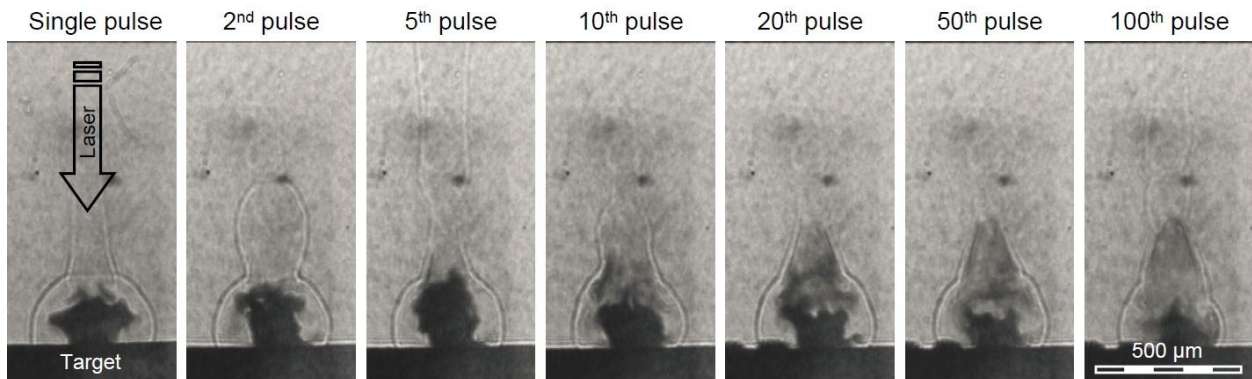


Figure 2-3: Resonance-absorption shadowgraphs of the material-vapor distribution and shock waves of plume generated by high repetition rate drilling of aluminum target. Other laser parameters: $\lambda=800\text{nm}$, $Q = 500\mu\text{J}$, pulse duration 500 fs [20]

The number of pulses hitting on a spot can have great influence on the generation and expansion of the plasma. Figure 2-3 shows the shadowgraph of the plumes captured for the last in a series of 500fs pulses with 1 kHz repetition rate. As can be seen from above figure, as the number of

pulses hitting a spot increases the hemispherical shock wave, cylindrical shock waves and material-vapor cloud each demonstrate a distinct behaviour. Although the hemispherical shock wave is little affected and maintains a symmetric spherical expansion even at high number of pulses, the vapor plume inside the shock wave quickly loses its symmetry and the vapor distribution become more and more turbulent at high number of pulses. In high pulse number regime, the geometry of the vapour cloud becomes less defined and the vapor mixes strongly with the atmospheric gas inside the shock wave resulting in the formation of eddies in the plasma flow.

Another example of plasma expansion is the commercial plasma spray torch used mostly in ambient conditions. The turbulent thermal plasma jets are attracting increasing number of applications for the plasma spray fabrication of coatings. However one of the factors that is greatly affecting their effective applications is the unavoidable entrainment of the surrounding cold gas into the plasma jets which can greatly alter the characteristics and quality of the final coating. Pfender et. al. conducted an analysis on the entrainment of cold gas into the thermal plasma jets of a commercial plasma spray torch [21]. They concluded that as the plasma jet exits the torch nozzle, it encounters a steep laminar shear at the outer edge of the jet as depicted in schematic of Figure 2-4.

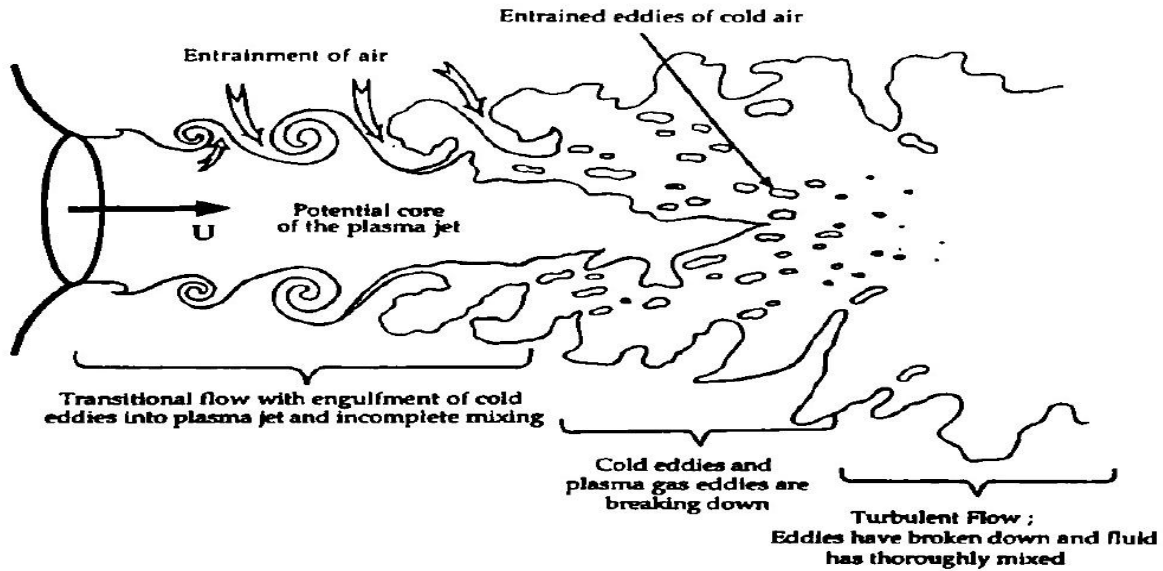


Figure 2-4: Schematic of a surrounding gas mixing into plasma jet generated commercial plasma torch [21]

The large velocity difference between the plasma species and the surrounding gas molecules induces the rolling up of the flow around the nozzle exit into a ring vortex which is carried downstream by the flow. As this vortex ring travel further downstream, the whole process repeats at the nozzle exist creating more vortices. As more vortex rings are formed they tend to coalesce with adjacent rings at the outer edge of the plasma jet forming larger vortices. Interaction of these vortices causes the instabilities around the entire ring resulting in distorted vortex rings that start entangling themselves with adjacent rings. Eventually these interactions ends in total breakdown of the vortex structures into large-scale eddies and the onset of turbulent flow. During this process the large amount of external air is engulfed into the plasma stream. The eddies of cold gas travel in the axial direction with much lower velocity and reaches the center line of the jet turning it to be completely turbulent along its entire length.

2.3 Summary

This chapter discussed the plasma expansion dynamics under various surrounding conditions. When the plasma is generated under a uniform pressure conditions, it expands outwards as two separate components: fast and slow. The fast component is mainly comprised of electrons, neutrals, and ions ejected from top few lattices of the target which travels with velocities of several km/s. Whereas the slow components expands with much slower velocity and it is comprised of nanoparticles and droplets that are directly ejected from the molten pool of target material. The expansion of these slow and fast components varies greatly with the change of surrounding pressure. At vacuum pressure, fast component has forward-directed motion, whereas the slow component is confined near to the target surface for much longer time. As the surrounding pressure increases, the fast component motion becomes spherical and more confined close to the target, while the slow component motion become forward-directed and overtakes the fast component at longer time delays. The nature of the background gas also greatly influences the character of the plasma expansion. If the background gas has much higher atomic weight than the of plasma species, the plume will be very confined and the expansion will be symmetric. If the plasma expands in background gas with light atomic weight, the interaction between plasma species and gas molecules will result in turbulent flow. The similar results were found when the plasma was created in ambient air. However, the main vapor ejected from target was enclosed inside the shock waves created by the breakdown of air due to interactions of laser pulse and plasma with surrounding air. It was discussed that when the plasma was created in such situation it was significantly influenced by various laser parameters. The plasma expansion transform from mushroom like symmetric expansion to rather turbulent behaviour inside shock waves as the pulse duration of the impacting laser is reduced from picosecond to femtosecond.

The similar result was also found when the number pulses hitting a spot were varied. Finally the interaction of plasma from commercial plasma spray torch with surrounding air was discussed. The velocity differences between the plasma species and the surrounding cold gas resulted in creation of vortices which resulted in the mixture of plasma eddies and cold gas eddies making the plasma expansion completely turbulent along the axis of plasma torch. The plasma expansion utilized for the experiments of the current research thesis, has the combinations of the surrounding conditions discussed in this chapter. For example, the target was irradiated in ambient air at an atmospheric pressure, but in the presence of the nitrogen gas flow which has very different velocity and low temperature. This resulted in a very unique complex plasma expansion generating very complex conditions for vapor condensation. The mechanism for vapor condensation will differ in different parts of the plasma; some places will have vapor condensation starting from homogenous nucleation while the other will result from the heterogeneous nucleation. The different nucleation process results in the generation of nanostructures with different size distribution.

Chapter 3: Experimental Setup

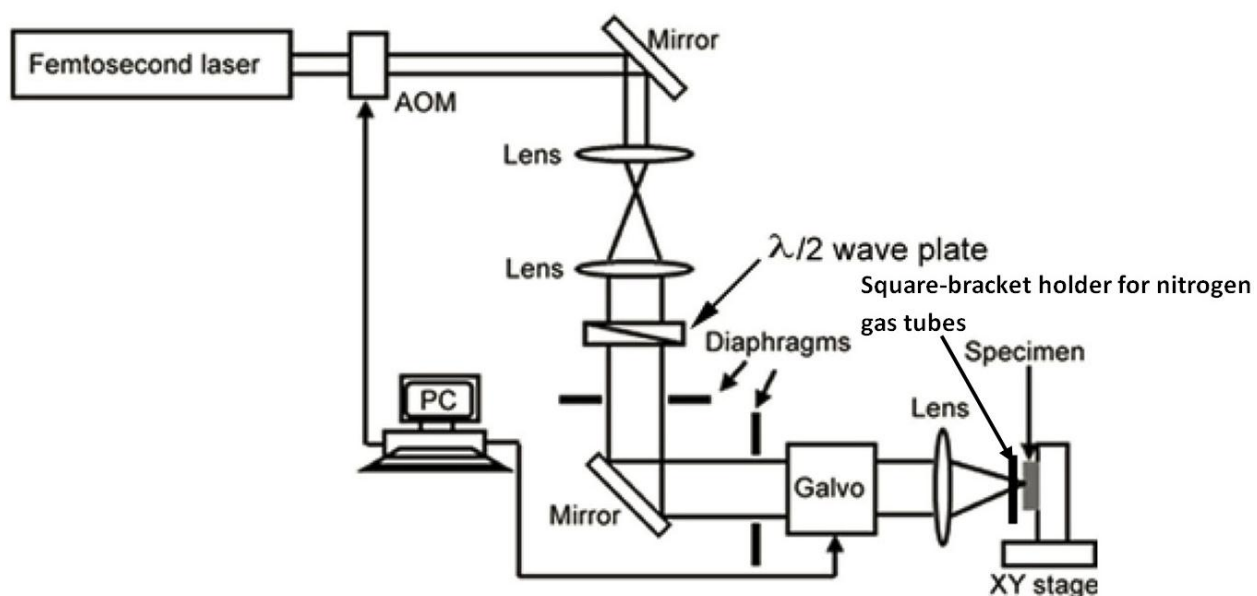


Figure 3-1: Schematic representation of the experimental setup

Figure 3-1 shows the schematic illustration of the experimental setup used in our study of femtosecond laser induced nanostructures on irradiated target sample. These experiments were performed using a direct-diode pumped Yb-doped fiber amplifier system ($\lambda = 1030$ nm) as laser source which has pulse repetition rate ranging from 0.2MHz to 26 MHz and a maximum average power output of 16W. The experiment was conducted on the samples of water-white microscopic slide glass which is composed of 60-75 % wt SiO_2 , 5-12 wt% CaO , and 12-18 wt% Na_2O . The samples' size was 1x1 inch with thickness of 0.90 – 1.10mm. The nitrogen gas flow was provided by six (Masterflex 6411.14) tubes arranged in a square bracket. The schematic of this arrangement is shown in Figure 3-2 as well as in Figure 3-1. The bracket is placed parallel to the target surface about 1-1.5cm apart. The tubes arrangement inside the bracket is such a way that the gas flowing from each tube collides with each other at the centre of the bracket and the

resultant gas flow is random and turbulent, and travel over the target surface. For all the experiments the nitrogen gas flow rate used was 5 SCFH (standard cubic feet per hour) and laser power used was 16W.

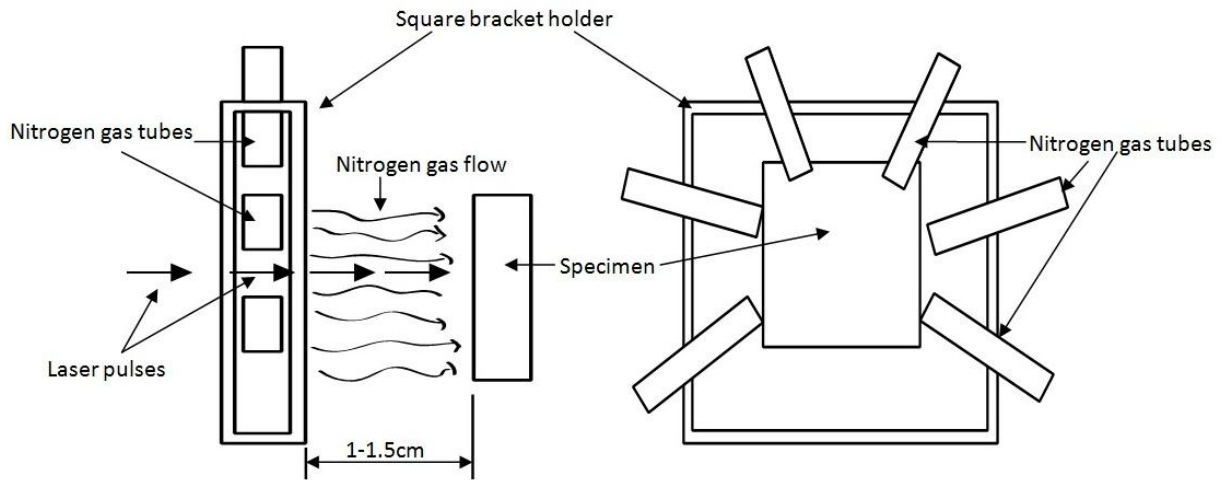


Figure 3-2: Arrangement of nitrogen gas tubes and specimen (Side view and front view)

For all the parameters the machining was done in the form of 26x26 arrays of micro-holes with a separation distance of 80 μ m between each hole. The very first experiment was done on two sets of sample for the pulse width of 214fs at 13MHz repetition rate and dwell time of 0.75ms to investigate the types of nanotips growth on the irradiated targets' surface. One sample was analyzed under x-ray diffraction (XRD) to determine whether the molecular structures of the generated nanostructures on sample surface was same as parent sample material or it had been altered; also to determine whether the nitrogen gas molecules get incorporated into the newly formed nanostructures from plasma condensates. The second sample was analysed under scanning electron microscope (SEM) system for the study of surface morphology; Energy Dispersive X-ray Spectroscopy (EDX) was done using the same system on second sample to determine the chemical composition of the nanostructures surface.

The study of nanotips generated under various conditions such as various laser pulse widths, repetition rates, dwell times, and polarization was also performed. The whole laser system is controlled by computer program, so the changing different laser parameters were easy. We investigated the effect of three different pulse widths (214fs, 428fs, and 714fs) on generation of nanotips for a repetition rate of 13MHz at a dwell time of 0.5ms. The effect of various laser pulse repetition rates (4MHz, 8MHz, and 13 MHz) and different dwell times was also investigated on glass samples. All the above aforementioned experiments were done using circular polarization of laser pulses. The quarter-wave plate was utilized in place of half-wave plate in front of the focusing lens to achieve the circular polarization. We also examine how the linear (p-) polarization would change the growth of nanotips of target surface. The linear (p-) polarization of beam was achieved by placing a half-wave plate in front of the focusing lens as depicted in Figure 3-1. For all the parametric study, only the SEM analysis was done on all samples for surface morphology.

Chapter 4: Proposed Growth Mechanism

4.1 Background Knowledge

Prior to understanding the mechanism of nanotips growth, we should first explore the reasons why there are size differences in the nanostructures generated with and without background gas flow in femtosecond laser ablation. According to the previous study done by our group, the size of the nanostructures generated with background gas flow is much larger than the nanostructures generated in absence of background gas [1]. This can be explained by the processes that are occurring when the plasma plume is expanding in background gas environment. These processes include expansion and deceleration of the ablated species, formation of shock waves, thermalization, recombination, clustering and particulate condensation [22, 23]. When the plume is generated, it expands in surroundings in two different components: Fast and Slow. The Fast component contains mainly the electrons, neutral atoms and single-charged ions which are relatively at high pressure and temperature. The Slow component consists of nanoparticles and fluidic droplets that propagate with a velocity which is two times smaller in magnitude compare to the fast component [17]. When the plume is generated in background gas environment with gas having certain flow rate in opposite direction, it becomes hard for the fast component to travel further in its direction at faster velocity. This creates the shock-wave front at the plume-gas interaction site which spatially confines the plume. The shock wave and the plume propagate radially and spatially outwards. In the case of plasma expansion under uniform gas pressure inside a chamber, the fast plume component is slowed down and reached by constituents of slow plume component [22].

However, when the femtosecond laser generated plasma plume is expanding in open air with opposing nitrogen gas with certain flow rate, the expansion mechanism is different to some extent. The results from the extensive investigation on the flow behaviour of a commercial argon plasma spray torch operating in atmospheric air can be utilized to explain this mechanism. As the plasma is generated and starts to expand outwards, the velocity difference between plasma and surrounding gas flow exert a steep laminar shear at outer edge of plasma. This creates vortex rings which travel downstream and towards the centre of plasma engulfing cold nitrogen gas eddies as well as eddies of plasma contents [21, 24, 25]. The velocity difference between these species creates turbulence in plasma expansion flow.

4.2 Nanotip Growth Mechanism

Due to this phenomenon, explained in section 4.1, that only occurs when the background gas flow is utilized in experiment, the velocities of plume constituents are greatly reduced and they come closer to each other and experience more collisions than without background gas flow. This reduction in plasma expansion velocities increase the plasma life time and thus plasma covers the irradiation spot for longer time which eventually effect the transmission of subsequent laser pulse to the specimen surface. Continuous generation of vortex rings at outer edges creates turbulences throughout plasma as it expands; eventually resulting in creation of more collisions and coalescing of adjacent eddies. As a result, larger clusters are formed in this scenario which eventually cooled into larger droplets and nanoparticles. These large plasma condensates get deposited back to the target surface resulting in larger nanostructures.

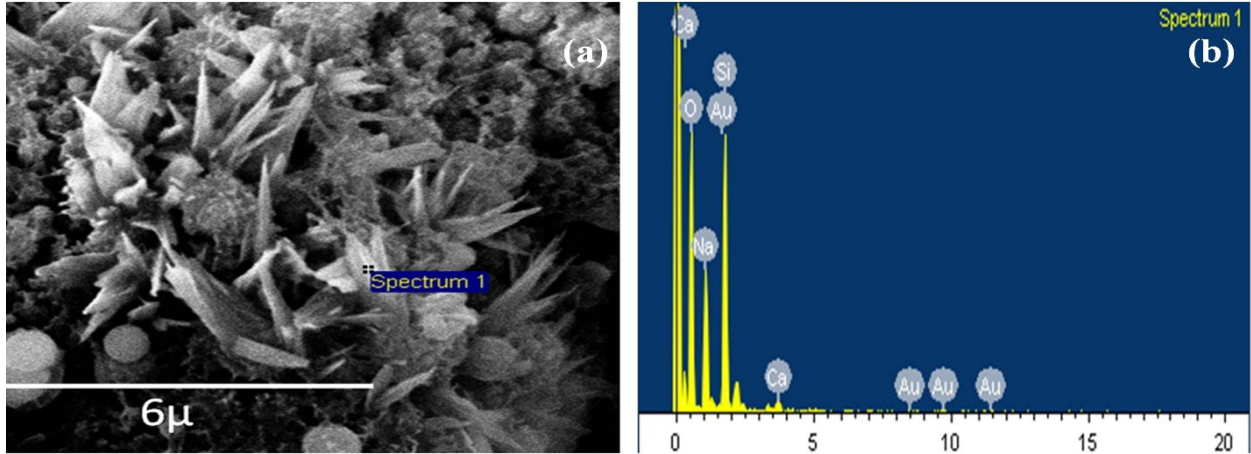


Figure 4-1: a) SEM image of femtosecond laser irradiated glass surface, b) corresponding EDX results

Figure 4-1 (a, b) shows the results of SEM and EDX analysis conducted on laser irradiated glass surface. Figure 4-1b shows the EDX analysis corresponding to nanotips shown in Figure 4-1a. As can be observed from these figures, there is no trace of nitrogen atoms in the nanostructures generated on the glass surface. This indicates that nitrogen does not take part, although it would promote, in nucleation and become part of the clusters formed in plasma vapor condensation.

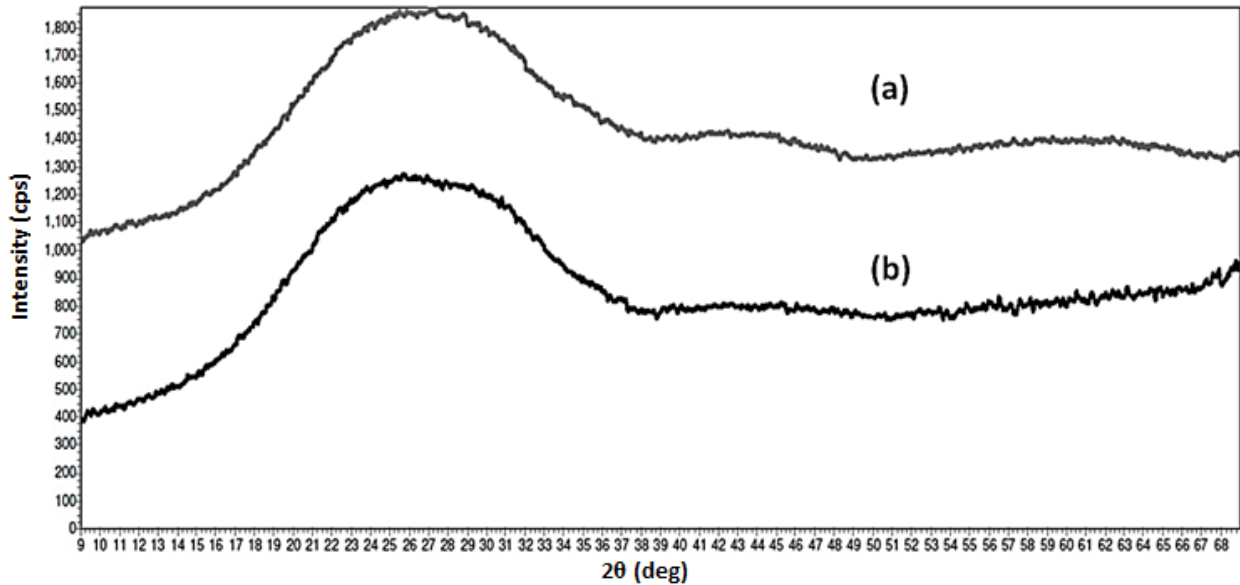


Figure 4-2: Comparison for XRD results of femtosecond laser a) non irradiated glass with no nanotips, b) irradiated glass specimen covered with nanotips

There is significant amount of gold atoms seen in EDX results. The reason for this is that the glass sample had to be sputtered with gold in order to make it conductive for SEM analysis. The XRD analysis was also conducted on laser treated and untreated glass surfaces. Figure 4-2 shows the comparison of XRD intensity graphs for treated and untreated samples. The laser irradiated glass surface is covered with nanotips; thus XRD is expected to show the structural difference between plain glass surface and nanotips covered glass surface. However, there is no intensity peaks observed in either of the graphs which shows that the sample structure is amorphous. Also both graphs follow same pattern which shows that there are no structural differences between the original glass sample and the nanostructures on irradiated glass surface. From the results of SEM, EDX and XRD analysis, it can be concluded that nitrogen gas role is limited to promoting the mixing of plume contents into larger clusters and cooling of the deposited droplets on irradiated target surface. It does not become part of the generated nanostructures.

The growth of the nanotips can be explained by the four processes which occur simultaneously. These processes are continuous generation of plasma plume, vapour condensation in plume, diffusion of nanoparticles, clusters and droplets from plume to the substrate surface, cooling down of the diffused plume species (nanoparticles, droplets). The generation process of plasma plume is different for different material. The transparent dielectric materials have very low laser absorptivity and wide band gap. As a result, only some part of the energy delivered by first few femtosecond pulses is absorbed via conductive electrons on the surface [8, 13]. Rest of the energy gets transmitted and refracted elsewhere. The conductive electrons absorb laser energy until certain threshold value; during which energy gets dissipated to adjacent lattice and gets accumulated as more laser pulses are delivered to the surface. This accumulated energy creates

colour centres, irregularities, microcracks on to the dielectric surface which increases the absorptivity of the irradiated surface [13, 15]. As a result, for subsequent laser pulses, greater portion of energy is absorbed. When the accumulated energy passes the conductive threshold energy for the electrons, it expulses the electrons, neutrals, and ions from the surface which makes the fast component of the expanding plume. The release of the electrons breaks down the bonds between the atoms in the top few lattices [8]. Due to the breakdown of the bonds, the lattices melt down and create pool of molten material as more energy is absorbed. The subsequent laser pulses along with shock waves eject the nanoparticles and fluid drops from the molten pool which makes slow part of the expanding plume.

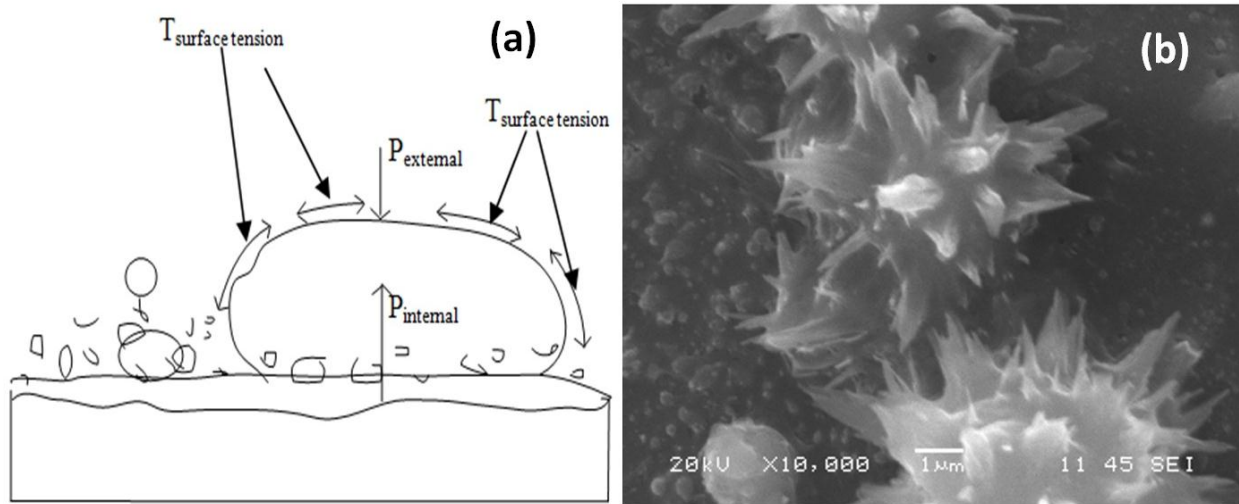


Figure 4-3: a) Schematic of the forces experienced by deposited droplets, b) SEM images of droplets with tips` stems (laser parameters: 214fs, 13MHz, 0.75ms dwell time)

During first few hundred pulses after starting of material breakdown, the content of the plume is very high and ideal to form larger clusters. These large clusters eventually diffuse from plume back on the target surface and become the stem for the growth of leaf-like nanotips. Since the plasma and nitrogen gas interactions result in turbulent flow, random amount of material from

vapor condensation is deposited arbitrarily over the target surface. As a result, the formed nanostructures have very wide size distribution; coalition of many clusters/droplets result in a larger droplet or a film of molten material, and isolated clusters/droplets forms an individual nanoparticles. The stem of the nanotips are initiated as the bumps resulted on deposited large/small droplets and deposited film of molten material as seen in Figure 4-3 and Figure 4-4.

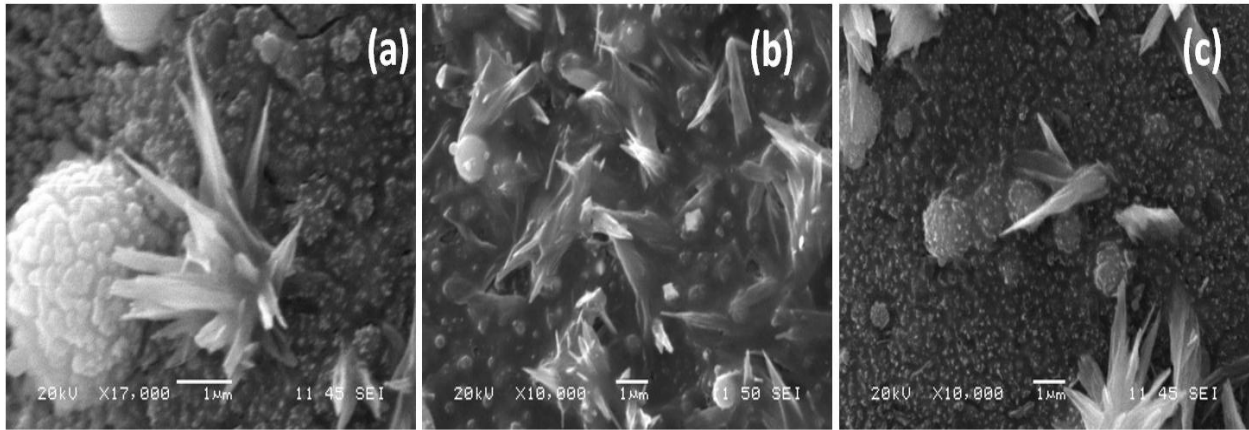


Figure 4-4: a) Types of tips formed after laser irradiation of soda-lime glass surface A) Flower like formation, b) Tips growth from deposited film of molten glass film, and c) Individual tip growth

These bumps are generated due to the combination of physical phenomenon that happens as the deposited molten material cools down. At first, the deposited materials land on the target which is at high temperatures due to the heat transfer from the laser-irradiated spot and radiation from plasma. Because the drop's bottom is in contact with hot surface, the particles adjacent to the hot surface experience high velocities inside the droplet creating upward motion inside the droplet. This creates internal pressure much higher than the external pressure experienced by the droplet due to atmosphere, gas flow, and plasma above the target. While these physical and thermodynamic processes are in action, the droplet is also being rapidly cooled by the random flow of nitrogen gas. Thus the top surface of the droplet experiences contraction which

eventually tries to reduce the volume of droplet. Since the nitrogen gas flow is not uniform over the droplet surface, the tension experienced by the surface is not uniform. This result in volume of material pushed out of the droplet from surfaces of less tension, which eventually forms stems for the growth of nanotips. The number of stems that grow from the deposited material depends on its volume. As can be seen from Figure 4-4a and Figure 4-4b, the larger droplets and deposited molten film can have multiple tips growing from them while the smaller droplet, Figure 4-4c, can have only one or two tips formed. But regardless of the volume of the deposited material, the stems will grow due to same physical and thermodynamic processes. The orientation of the tips is mainly expected to be governed by the surface tension. Where ever there are regions of relatively less surface tension, the material from within deposited volume will try to escape outward from these spots. The surface tension is a function of cooling rate which is dependent on the nitrogen gas flow. The nitrogen gas flow is random over the target surface which eventually results in formation of tips in random directions.

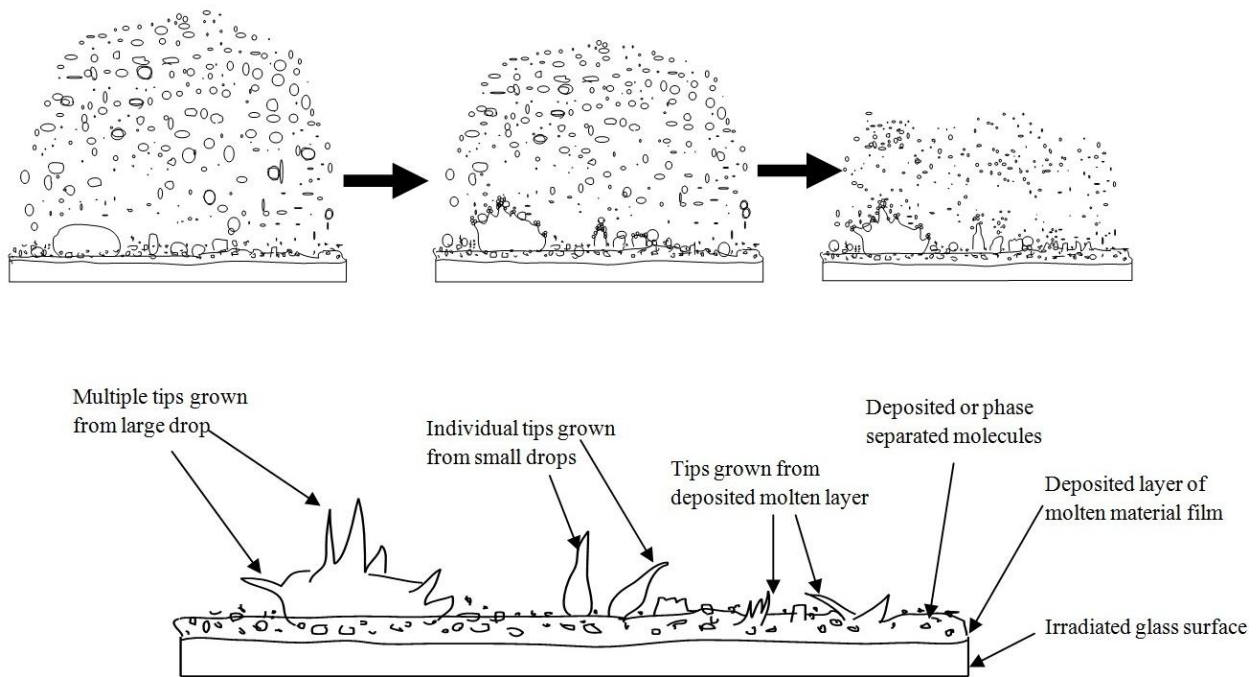


Figure 4-5: Schematic for growth steps of nanotips

Figure 4-5 depicts the steps involved in the growth of the leaf-like tips. While the stems grow from deposited material, more and more droplets/nanoparticles condense out of the plume and land on the stems. If the stem is still hot, not completely cooled into solid state, the landed droplets dissolve into the stem to become part of the volume. This volume, as more droplets arrive, grows in the direction of the orientation of the stem. As can be seen from Figure 4-3 and Figure 4-4, the cross section of this volume of tips reduces while it is growing in length. This reduction in cross section, due to which these structures are called nanotips, is the result of two different processes: generation of smaller and smaller droplets as tips grow and the thermal variations in soda-lime silicate glass.

The formation of smaller droplets/nanoparticles is due to the absorption of laser pulse energy by plasma. Once the breakdown threshold for soda lime glass is reached and the plasma is created, the irradiated spot gets covered by the plume content. As discussed above, when plasma is expanding in nitrogen gas flow environment, its life time increases to few hundreds of microseconds which is much larger than the time delay between two laser pulses (76.92ns for 13MHZ). Consequently the plume content reflects, absorbs, and diverts some of the pulse energy away from the focus spot. As a result, only a portion of the pulse energy is transmitted from subsequent pulses to the target, resulting in smaller amount of target material being ejected to the plume. As time and number of pulses increases, there is less content added to the plume which means that the mean free path for eddies trapped inside turbulent plasma become wider and wider resulting in fewer collisions between eddies. This causes the formation of smaller clusters. As the proof of this phenomenon, it can be seen in Figure 4-4a and Figure 4-4c that the target surface is covered with white dot-like nano-sized particles which are formed later in time and has

same size range as the narrow end of the tips. These white dot-like nanoparticles are not visible in Figure 4.4b; they might have been remelted because of the high temperatures of the deposited film and became part of the film volume. Another phenomenon that contribute to the reduction of the cross sectional area of the tips is the silicate part of the Soda lime silicate glass. More than 50% of the composition in soda lime silicate glass exists as silicates' randomly oriented tetrahedral networks. This vitreous silica glass networks experience a negative thermal expansion between absolute zero and the room temperature which is exactly the case in this experiment [26]. The droplet and particles that are deposited to the target surface have high temperatures because of the plasma and heat diffusion from irradiation spot to outward in the target. As these droplets, particles and growing tips structures cool down due to nitrogen gas flow, they experience shrinkage of volume. This contraction of volume is mainly due to the transverse oscillations experienced by the bridging oxygen of adjacent silica tetrahedral. As the temperature of the silica glass goes down, the oxygen connecting two tetrahedra transversely oscillates with mean amplitude, A , which has magnitude of about 28% of the Si-O bond length [26]. This results in decreased distance between two adjacent tetrahedra resulting in contraction of the whole volume. The following chapter discusses the influence of laser parameters on the growth of leaf-like nanotips on the target surface.

4.3 Summary

The growth mechanism for the nanotips has been explained in this chapter. When plasma expands outward in presence of background nitrogen gas flow, the turbulences are generated in flow due to the interactions between plasma species, nitrogen gas molecules and laser pulses. The turbulences promote more collisions among plasma species resulting in formation of large

clusters and droplets in plasma. When plasma condensates get deposited to the hot target surface, they experience the imbalance of forces due to temperature and pressure differences between hot target and surroundings. This results in initiation of stems on the surface of deposited plasma material upon which more plasma condensates continuously get deposited. As more material is added, the nanotips grow in the direction of the stems. The reduction of the nanotips' cross section along the length is attributed to two factors; one due to the continuous generation of small droplets from plasma condensates, and second due to negative thermal expansion experienced by the silicate networks of soda-lime silicate glass structures between absolute zero and room temperature as hot nanotips' structure cools down.

Chapter 5: Influence of femtosecond laser parameters on growth of nanotips

5.1 Effect of pulse width

There are two mechanisms responsible for laser-induced optical breakdown of materials: multiphoton absorption and avalanche ionization. Multiphoton absorption results when a molecule absorbs required amount of photons simultaneously to get ionized and it is proven to be the main mechanism for breakdown in the low-femtosecond regime [27]. In the current experiments, the investigated pulse widths fall above low regime where the combination of both mechanisms is believed to be responsible for the breakdown. The multiphoton ionization is responsible for initial generation of electrons which are further heated by incoming portion of the pulse resulting in avalanche ionization and rapid plasma formation [28]. However, both breakdown mechanisms require laser intensity in interaction volume to reach a minimum- though different- threshold value in order to start target breakdown. The initial part of pulse produces free-electron plasma which can absorb the later part more efficiently and/or behave as mirror and reflect most of the incident energy [27, 29, 30]. Every material has its unique optical damage threshold fluence, but all the pure dielectrics demonstrate similar behaviour in all range of pulsewidth as observed for SiO₂ [31]. Stuart et al. investigated the threshold fluence for fused silica and CaF₂ with laser pulses in the range $270 \text{ fs} \leq \tau \leq 1 \text{ ns}$ [31]. They discovered that the damage threshold decreased with the decrease of the pulsewidth.

Although, this research was focused on pulses in femtosecond regime (214fs-714fs), the findings in Stuart et al. investigation are more relevant to these experiments as they worked with multiple

pulses of laser with wavelength of 1053nm in order to measure the damage threshold for SiO₂ [28]. However, they have not mentioned the exact number of pulses or the laser pulse repetition rate they used in their investigation. Thus, it is assumed that the pulse repetition rate (13 MHz) and the number of pulses (6500) we utilized are much greater than what they might have used. Both high laser pulse repetition rate and high number of pulses is responsible for comparatively high thermal accumulation in target. Hence, whatever results Stuart et al. achieved between picosecond and femtosecond pulses, in this work it is acquired within femtosecond pulse regime. For example, they discovered that the damage area generated by the 500fs pulse in fused silica glass was twice as much smaller than that produced by the 900ps pulse. Even though this research did not involve working in picosecond pulse length regime, similar result were obtained as the pulse width increased in femtosecond laser pulsewidth range. Figure 5.1 shows the SEM images of the micro holes drilled by femtosecond laser pulses at 13MHz frequency for 0.5ms dwell time with pulse widths of 214fs and 714fs respectively. The diameter of these micro holes is approximately on average 12μm and 21μm respectively. The size of micro-hole represent the amount of material removed from the target; larger diameter means larger amount of material removal compare to smaller hole diameter.

Fan and Longtin developed a femtosecond breakdown model which gives the time at which the laser intensity reaches the breakdown threshold at a given position [27], $T_B(Z)$.

$$T_B(z) = \frac{z}{c} \pm \tau_P \sqrt{\frac{1}{4 \ln 2} \ln \left[\beta \left(1 + \frac{z^2}{z_R^2} \right)^{-1} \right]} \quad (1)$$

Where z is axial location in focal region ($z=0$ at focal point), τ_p is Full Width at Half Maximum pulse duration, c is the speed of light in the medium, β is the ratio of peak pulse power to the breakdown threshold of a material (P_{\max}/P_{th}), Z_R is the Rayleigh range or focal region ($= \frac{n\pi w_0^2}{\lambda}$).

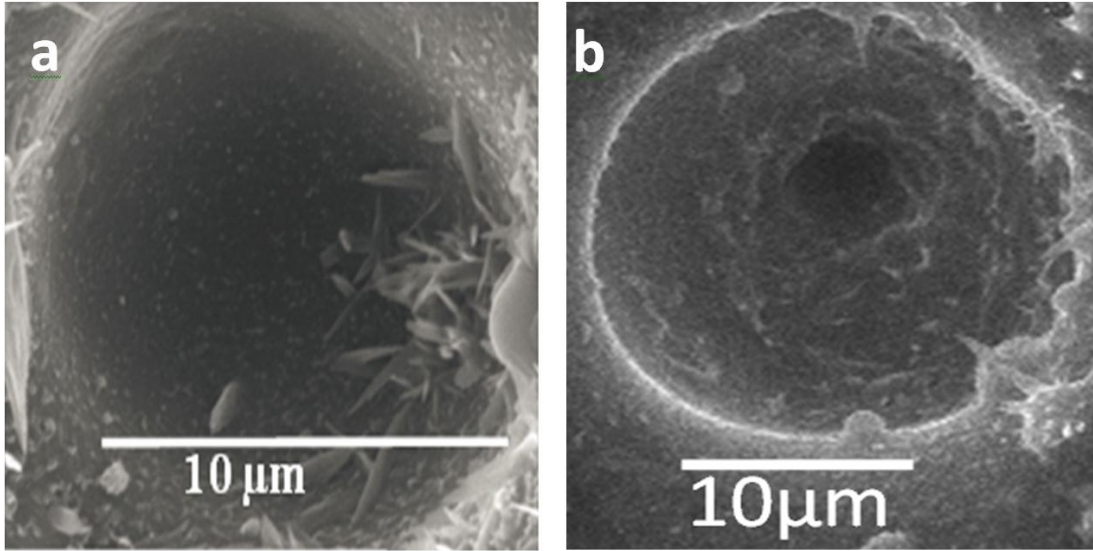


Figure 5-1: Micro holes drilled by femtosecond pulses with pulse width a) 214fs and b) 714fs

Equation 1 gives the time at which breakdown starts after the laser pulse started interacting with target surface at a given position in focal region. From this point in time onwards, plasma starts to grow, expand, and covers the irradiated spot for several nanoseconds during which the second part of laser pulse is still travelling towards the target surface. Using this equation the time required for breakdown is calculated to be 77fs, 189fs, and 325fs for pulse width of 214fs, 428fs and 714fs, respectively. Longer is the time spent by the pulse travelling through the plasma, greater is the amount of energy lost to the plasma before reaching to the target. Short laser pulse (214fs) reach threshold fluence very early since they possess high intensity. However they are very short and thus spend less amount of time in plasma and loose less energy to the plasma

compare to longer pulse ($>214\text{fs}$) and thus it removes target material more efficiently than longer pulse. Hence, as can be seen from Figure 5-1a), the hole ($\sim 12\mu\text{m}$ diameter) drilled by 214fs pulse is more close in size to the spot diameter of $10\mu\text{m}$ of laser.

Regardless of the size of the pulse width, the ablation of irradiated target only starts when pulse intensity reaches the breakdown threshold. However, more important is the time of the pulse used to produce the plasma once the breakdown has started and the amount of time pulse travel through the plasma. Since shorter pulses spend less time in plasma, most of their energy gets transmitted to the target surface to remove the material efficiently. On the other hand longer pulses spend significant portion of pulse duration travelling through previously formed plasma. Also the turbulences created in plasma due to nitrogen gas and expanding plasma interactions lengthen the plasma life. As a result, energy transmitted via longer pulse is not enough to ablate the material upon contact with the target material. Rather this transmitted energy gets stored in top few lattices and get transferred to bulk lattices in all direction which make the target temperature rise in irradiated spot surrounding area, and make molecules to become loose to form larger pool of molten material. As a result, the subsequent longer pulses expulse large particles and larger droplets into the plasma upon contacting the molten pool; on contrary during interaction of short pulse with target surface does not cause as much high temperature rise which causes shallow molten pool upon interaction of shorter pulse. Hence, during short pulse the material removed from the target is composed of smaller particles, and droplets.

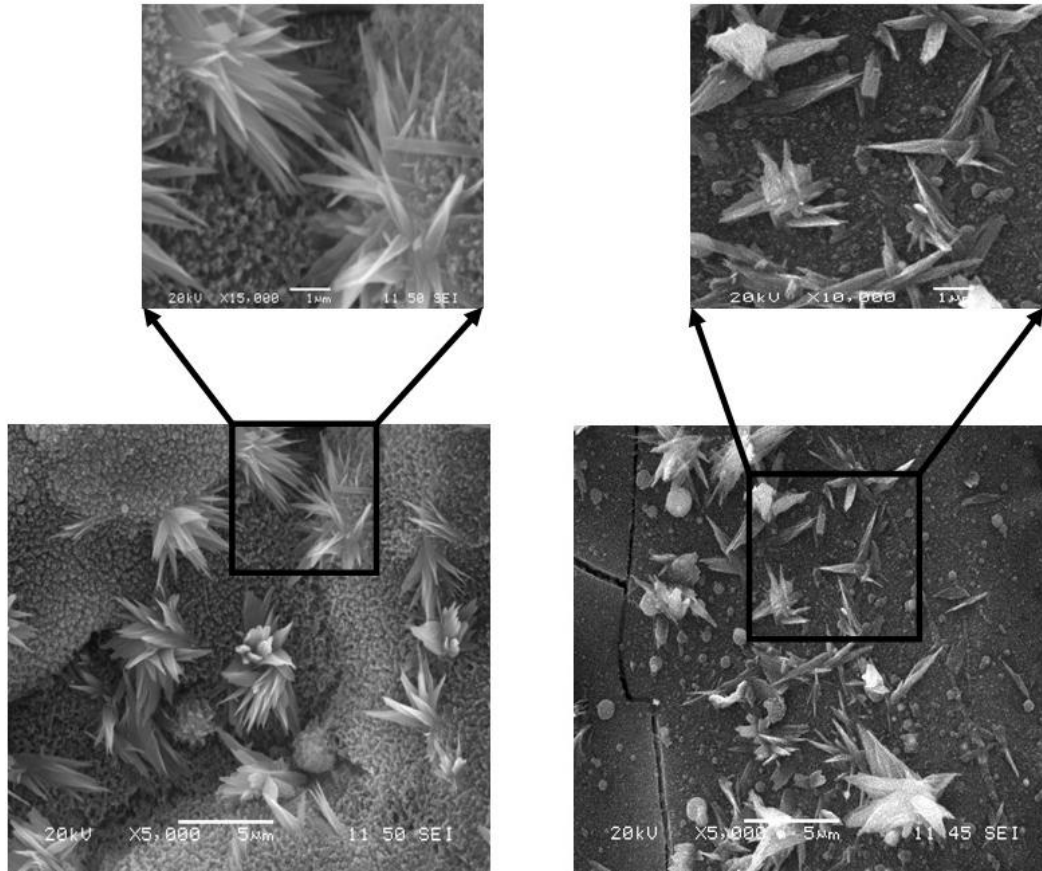


Figure 5-2: Tips generated at 214fs for 13MHz at dwell time of 0.5ms

Size of the plasma species and the temperature rise of the target surface greatly affect the type of nanotips that grow on the target surface. The growth mechanism responsible for leaf-like nanotips generated for 214fs laser pulses with background of nitrogen gas flow has been explained in chapter 4. For 214fs laser pulses at 13MHz, we reported three kinds of nanotips growth: individual tips from single droplet, multiple tips from single large droplet forming flower-like arrangement, and multiples tips grown from molten film of ablated material. Figure 5-2 shows the SEM images of randomly selected spots from irradiated target surface with 214fs laser pulses; only the individual and flower-like nanotips formations are shown here as most of the irradiated area was covered by these two types of nanotips. There were very few areas with

nanotips growing from film of molten material. A very interesting pattern is observed in terms of types of nanotips grew according to the pulse width. When laser pulse width was increased from 214fs to 428fs and 714fs, only the nanotips formed from molten target film material or large droplets were found to be growing on target as observed in Figure 5-3 SEM images.

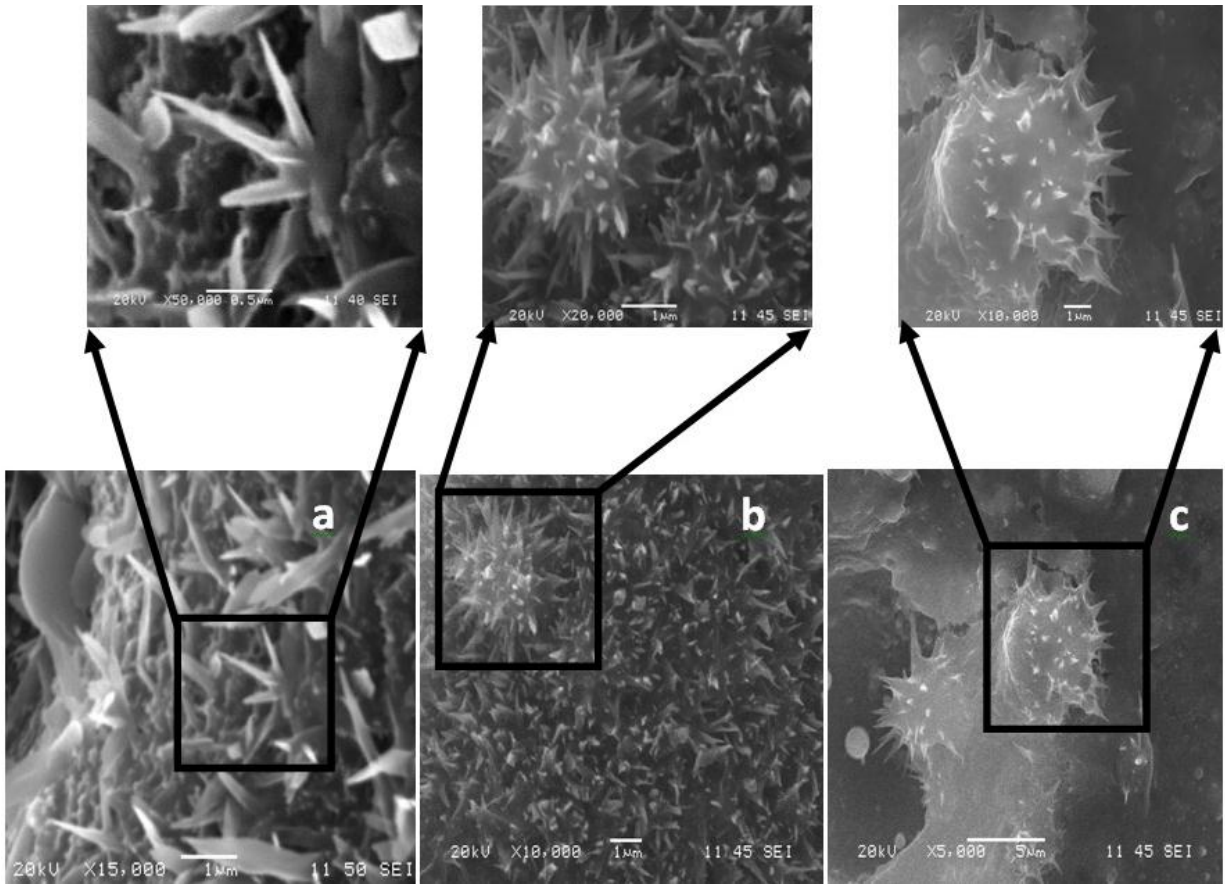


Figure 5-3: SEM images of nanotips grown in target irradiated with a) 214fs, b) 428fs and c) 714fs laser pulses

As explained earlier, longer pulses create larger molten pool and the plasma species is mainly comprise of larger particles and large droplets. Breitling, et al. performed the vapor flow analysis of plasma created on aluminum target under ambient atmosphere. Their study revealed that the vapour-plasma expansion is much more like regular mushroom-cloud for longer pulses,

whereas it is more turbulent for the shorter pulses. This is mainly due to the disturbances caused by much longer propagation length and nonlinear radiation-gas interactions for short pulses [20]. In this study, the nitrogen gas flow generates extra turbulence in expanding plasma. As a result, the already large particles and droplets experience collisions with other large species resulting in formation of larger droplets which upon deposition back onto target surface spread into film. The longer pulse creates high temperature in target surface which result in most of the droplets being spread into film even before nitrogen gas cools them down in their original shape. There are still chances of forming smaller droplets in the plasma vaporization since plasma species interaction is very random. However, the smaller droplets are most likely to get dissolved into surface molten layer because of the higher target surface and molten film temperatures. At 428fs pulse width as seen in Figure 5-3b), there is significant number of nanotips growing from molten film. However when the laser pulse width was further increased to 714fs, the number of nanotips growth is found to be very small even though it formed from molten film as depicted in Figure 5-3c). This might be due to the fact that during 714fs pulse interaction of target surface, it must be creating very large amount of molten material which get ejected into the plasma as well as pushed around the drilled hole due to shock waves in plasma. As a result, very short nanotips are observed to be growing from relatively large liquid volume of molten glass as seen in Figure 5-3c).

5.2 Effect of laser pulse repetition rate

Three different pulse repetition rates (13 MHz, 8 MHz, & 4 MHz) were tested for this study. As the repetition rate reduces, the time separation between two pulses increases which eventually changes how the pulse energy is being transferred into the target and being used to remove the

material out of the target. If the time gap between two pulses is less than the time required for heat to diffuse out of the focal volume for a typical glass, then the heat will accumulate from subsequent pulses in focal volume and elevate the target temperature which moves outwards on surface and into the bulk. The characteristic thermal diffusion time in glass is about $1\mu\text{s}$ for a volume of $0.3\mu\text{m}^3$ [32]. This thermal diffusion time will vary from glass-to-glass according to their compositions; which could make another topic of extensive research. However for this report, this value is taken as a reference. In comparison to this thermal diffusion time, the separation time between two pulses is much smaller; 77ns, 125ns and 250ns for 13 MHz, 8 MHz, and 4 MHz repetition rate, respectively. Even though, all the aforementioned time is much less than heat diffusion time of $1\mu\text{s}$, the heat accumulation will be high in and around focal volume at high repetition rate compare to low repetition rate. As a result, the energy per pulse required to start breakdown reduces as the pulse repetition rate is increased. This breakdown threshold energy per pulse is found to be $2.0315\mu\text{J}$, $1.3375\mu\text{J}$ and $0.8615\mu\text{J}$ for 4 MHz, 8 MHz, and 13 MHz, respectively. However, the laser machining in our experiment was done using a maximum average power of 16W which provided the pulse energy much higher than the threshold energy required for each individual repetition rates. As a result, the temperature elevation in laser-target interaction zone is very high for each increasing repetition rates. As the repetition rate is increased the size of the tips and the number of tips growth varies as seen in Figure 5-4. It is obvious from Figure 5-4a, that for 4 MHz repetition rate, very few nanotips grew on random places, whereas for 8MHz and 13MHz nanotips grew with high number of density over the large surface as seen in Figure 5-4b and Figure 5-4c. However, the nanotips grew on surface irradiated with 13MHz are much larger narrow leaf-like compare to the tips grew on target surface irradiated with 8 MHz pulse repletion rate. These changes in nanostructures can be explained by

how the material is removed from the target surface for each repetition rates, and how the subsequent incoming laser pulses interact with plume of ablated species.

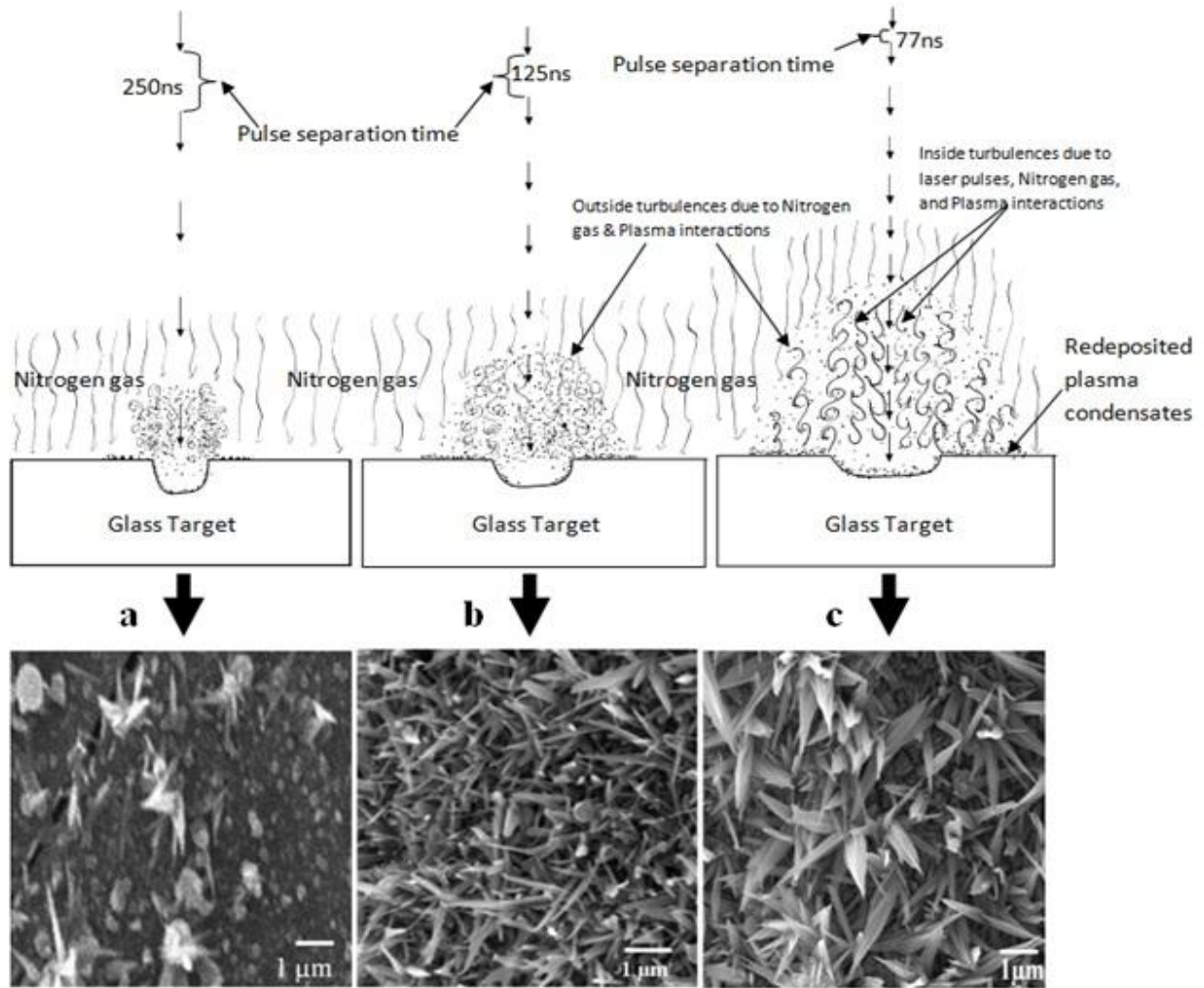


Figure 5-4: Nanotips generated for the average laser power of 16W for pulse repetition rates of a) 4MHz, b) 8MHz, and c) 13MHz; the dwell time was 0.5 ms for all three cases

High repetition rates provide more number of pulses hitting the same spot for a given dwell time in comparison to lower repetition rates. In this case, the dwell time was 0.5 ms which provides 6500 pulses, 4000 pulses, and 2000 pulses for repetition rate of 13MHz, 8MHz, and 4MHz, respectively. As result, for each progressive number of pulses a much larger of volume than the focal volume is heated above the melting temperature for the glass and much larger radius of

glass melts on the surface [32]. As a result, the plume generated at higher frequency is much wider and last in air for longer time as depicted in schematics of Figure 5-4 corresponding to each repetition rate. At higher number of pulses interaction, the vapor distribution inside the plume rapidly loses its symmetry and becomes more and more turbulent [20]. These turbulences in plasma expansion are generated due to two different kinds of interactions. The turbulences generated at the outer edges of the plasma are the results of the interactions between incoming nitrogen gas flow and the outgoing plasma species. Whereas the turbulences in core of the plasma are resulted due to the interactions between the highly energized plasma species from incoming laser pulse absorption and nitrogen gas molecules which might have entered the plasma core. Due to the turbulent interactions, the plasma species expand wider and thus the redeposition back to the target surface occurs over larger surface area resulting in much more number of nanotips. When the ablation is done at 8MHz repetition rate, the plasma must have ideal condition in terms of the amount of the turbulence and ablated material available which lead to the growth of high populated and oriented nanotips which are narrower than nanotips generated at 13 MHz. The plasma has excessive material and more violent turbulences when the machining is done using 13 MHz repetition rate. This results in growth of nanotips which are much wider leaf-like and more randomly oriented compare to 8MHz. For low number of pulses, the plasma expansion and interaction with surrounding nitrogen gas is less turbulent. Thus the plasma does not expand out ward as much resulting in plasma species being closer. Since the vapour contents are much closer they will result in larger droplet rather than resulting in small droplet being deposited over large surface area. As a consequence, only few nanotips are found to be growing randomly from large droplets for 4MHz repetition rate as can be seen from Figure 5-4a.

5.3 Effect of dwell time

The dwell time study was performed for 214fs pulse width and 8MHz repetition rate. The Figure 5-5 shows the SEM images of the glass target machined with dwell time of 0.1ms, 0.25ms and 0.5ms. The growth steps of the nanotips are clearly evident from these three images. At 0.1 ms the plasma has very little vapor contents which results in the redeposition of the droplets on the target surface and the stem growth for the nanotips is seen in Figure 5-5a. As the dwell time is increased to 0.25ms and 0.50ms, the generated plasma become more and more dense as the more material is ablated from the target due to more number of interaction pulses. Once the stem growth for the tips started on the target surface, then the continuous redeposition of vapor condensates from plasma back to surface provide building material for tips to grow. It is clear from Figure 5-5 that the growth of these nanostructures is dependent on the dwell time as much as other laser parameters. For example for 0.25ms dwell time, the plasma has just enough building material for tips to just start growing in nanoscale to a micrometer length; the number of tips present on surface also increased. When the dwell time is further increased to 0.50ms for 8MHz repetition rate, it is evident from Figure 5-5c that nanoscale tips grew to the length of 1-2 μ m and the target surface is densely populated with nanotips over large area. The ablation mechanism somewhat changes from one repetition rate to another due to the different threshold energy per pulse requirement for each pulse.

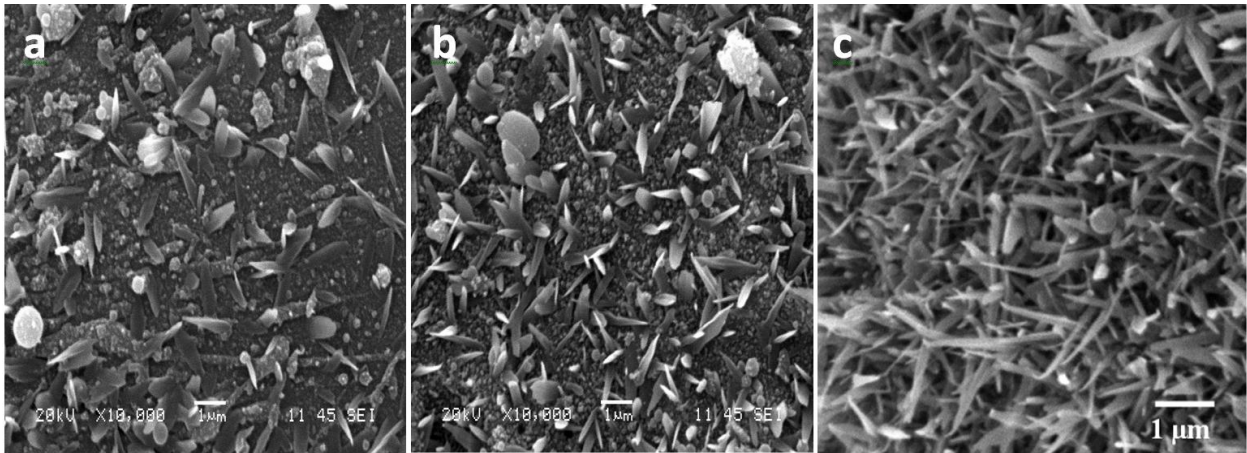


Figure 5-5: Nanotips growth stages at 8MHz repetition rate for dwell times of (a) 0.1ms, (b) 0.25ms, and (c) 0.50ms

The incoming pulses also interact differently with plasma generated from previous pulses for each repetition rate. Thus the nanostructures generated for even the same dwell time differs for each repetition rate as seen in Figure 5-4 and Figure 5-6. However for each repetition rates, the nanotips will grow only up to certain dwell time. If the machining is continued beyond that particular point, the nanotips growth for each repetition rate is greatly hindered. Figure 5-6 shows the SEM images of the glass target irradiated with 4MHz, 8MHz, and 13MHz repetition rates for the dwell time of 0.75ms. As can be seen for each of the repetition rates, the number of nanotips produced is much less than what was achieved for 0.50ms as seen in above Figure 5-4. Instead the present of lots of spherical nano-microparticles and molten droplets are observed. The reason for this drastic change is that when machining is continued beyond certain dwell time, the extra pulses that travel through the plasma heat up the plasma species to higher temperatures as well as they add extra ablated material from the target plasma. This phenomenon can better be understood from the schematic representation depicted in Figure 5-7.

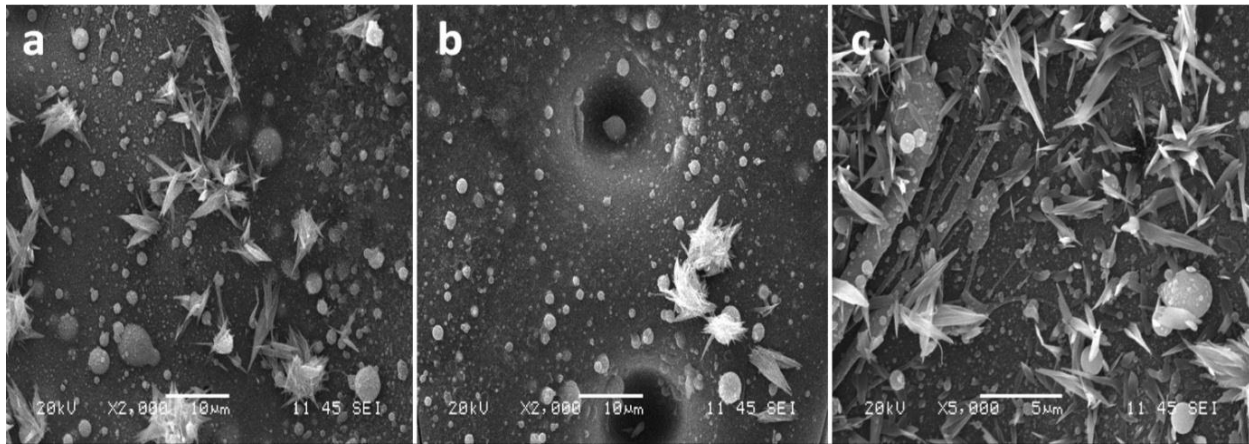


Figure 5-6: Nanostructures generated at dwell time of 0.75ms for the repetition rate of (a) 4MHz, (b) 8MHz, and (c) 13MHz

The effect of high number of pulses on the growth of the nanotips is demonstrated in form of four intermediate stages in Figure 5-7. It is clear from the above figures that the repetition rate and dwell time affect the growth of nanotips in somewhat similar way. The reason for this could be that both the high repetition rates and high dwell time provide number of pulses much higher than required to ablate just enough material from target to initiate and complete the growth of nanotips. For the tips to initiate and grow, it requires the force imbalance and just enough material to finish the growth. When the breakdown of the target material starts, it required certain number of pulses according to the repetition rate or the dwell time to ablate required amount of target material into the plasma as demonstrated in Stage 1 to Stage 3 in Figure 5-7. Before this point in time, the plume does not have enough plasma monomers to start vapour condensation. Once the vapor condensation starts inside the plume, the vapor condensates start getting deposited onto the target surface where they come in contact with hot target surface as depicted in Stage 3. If the machining is stopped at Stage 3, there will not be any more incoming pulses that transfer energy to plasma species to generate further turbulences. As a result, the plasma species start relaxing by mixing with nitrogen gas molecules and cooling down. The

consequence of these phenomena will be that the pressure exerted on the redeposited plasma condensates on target surface by above plasma species will be relieved. Furthermore due to the hot target surface, the redeposited material experience internal pressure much higher than the external pressure. This imbalance of pressure pushes the material out of the volume of deposited droplets resulting in the formation of the stems for the nanotips as depicted in side figures of Stage 3 in Figure 5-7.

However when the irradiated spot is bombarded with too many pulses as in the case of high repetition rates and high dwell time, too much material is added to the plasma and the incoming subsequent pulses interact with plasma species elevating their temperature and giving them high kinetic energy. As a result, the plasma expands outward faster and to the larger radius exerting the more pressure in surrounding including to the redeposited plasma vapour condensates on target. This creates the external pressure approximately similar to the internal pressure of the redeposited material, hence hindering the formation of stems upon which the tips could grow, Stage 4 of Figure 5-7. The excessive temperature of the plasma species and the target can also remelt the deposited material as well as previously grown stems and tips. The SEM image of the target irradiated with 8MHz repetition rate for the dwell time of 0.75 ms depicted in Figure 5-6b is the perfect example of the stage 4 illustrated in Figure 5-7. For 8MHz repetition rate at 0.75ms dwell time, most of the redeposited material must be experiencing approximately equal internal and external pressure resulting in formation of just circular nano-micro particles rather than the formation of stems. There is evident of formation of few very tips from bulk droplets in Figure 5-6b.

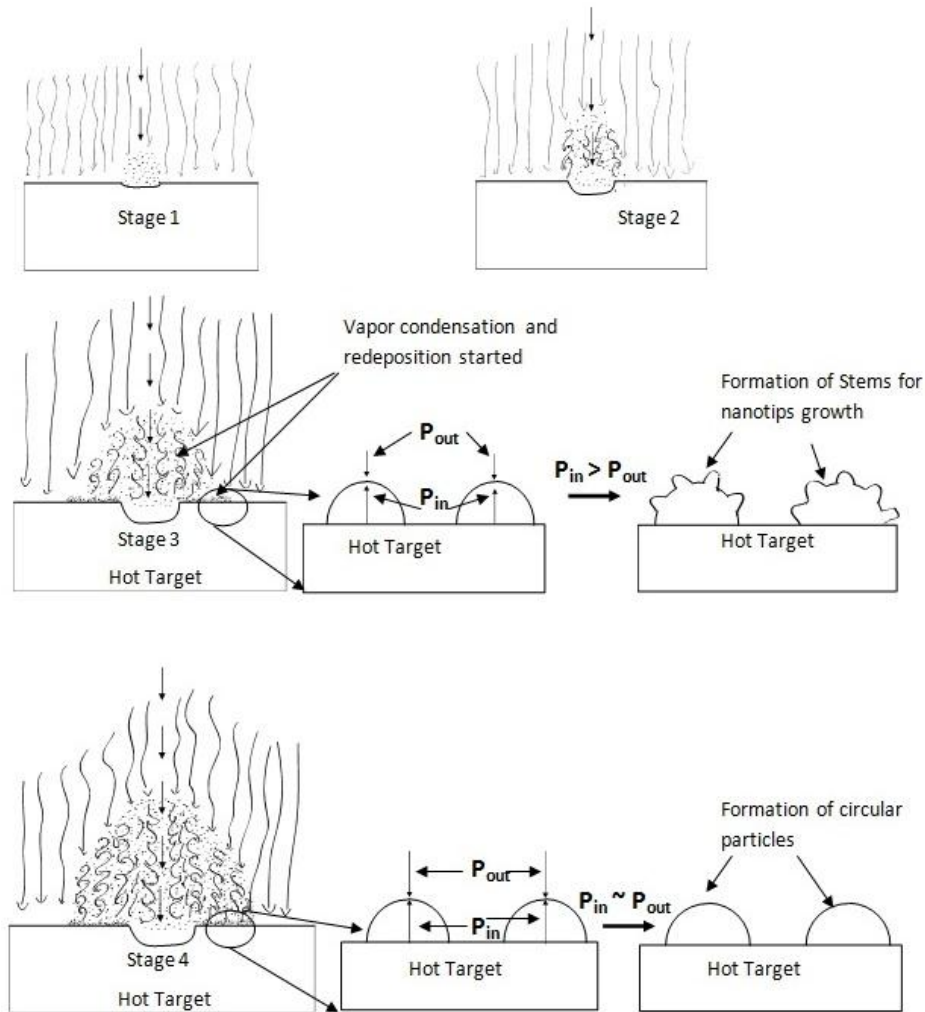


Figure 5-7: Growth stages of plasma expansion and nanotips formation

Surprisingly if we follow above four stages, there should not be any tips growth for 13MHz repetition rate for the dwell time of 0.75ms. However from Figure 5-6c, it can be seen that significant number of nanotips grew on the target. This shows some nonlinearity between the tips growth and the femtosecond laser parameters. This nonlinearity can be explained by the behaviour of the plasma expansion. The 13MHz provide much more number of pulses in comparison to 8MHz and 4MHz for the same dwell time. As a result for 13MHz, the machining is done way beyond stage 4 of the growth mechanism. When the plasma reaches stage 4, it will

exert excessive pressure and temperature on previously deposited material resulting in remelting and formation of nano-micro particles. But at the same time since plasma is continuously being heated by incoming pulses, it will rapidly expand outward. There will be a point in time where the plasma has expanded far enough from the redeposition site relieving excessive pressure and temperature. From this point onward, the transmission of the subsequent laser pulses will improve and the new material will be ablated from target forming new plasma over the target surface. This whole phenomena must be occurring in the last part of 0.75ms dwell time during which the growth mechanism start back at Stage 1 and from nanotips on previously deposited material as seen in Figure 5-6c.

5.4 Effect of laser polarization

All the experiments discussed above were done using circular polarization of femtosecond laser. Investigation was also carried out to test whether the linear polarization changes the growth mechanism of nanostructures on the laser irradiated target glass. The effect of laser polarization on the ablation of various materials has been studied by many researchers. Hee et. al. [33] studied the effect of polarized femtosecond laser pulses on the generation of relief gratings on (111) silicon substrate using a novel interferometer. The ablation was done by focusing two interfering femtosecond laser beams under different polarization combinations. In their investigation, they found that p:-p-polarization has the lowest ablation threshold and generates the deepest grating depth among other polarization combinations (s:- s-polarization; c:- c-polarization). Camacho-Lopez et. al. [34] investigated growth of grating-like structures on titanium films using circular (c-) and linear (p-) polarization. They discovered that there was no formation of grating-like structures when the substrate was irradiated with circularly polarized

light. However, when the linearly polarized laser pulses were utilized, the grating-like structures were generated at the fluence well below the ablation threshold for Titanium film. Furthermore, Venkatakrisnan et. al. [35] also found in their study of polarization effect on ultra-short pulsed laser ablation of thin metal films that the linear (p-) polarization has the ablation threshold less than that for the circular polarization. In our investigation we found results that support the findings in aforementioned investigation done by other researchers. We found that when the glass was irradiated using p-polarized laser pulses, much more number of nanotips found to be growing for the same parameters in comparison to circularly polarized pulses as depicted in Figure 5-8. It was found by other researchers that the p-polarized laser pulses ablate target material at fluence much smaller than the ablation threshold fluence for circular polarization. If this is true then the p-polarized pulses remove material much more efficiently with much less number of pulses in comparison to circularly polarized laser pulses. In other words, the growth stages explained in Figure 5-7 must be occurring in fast-forwarding mode during linearly polarized laser ablation.

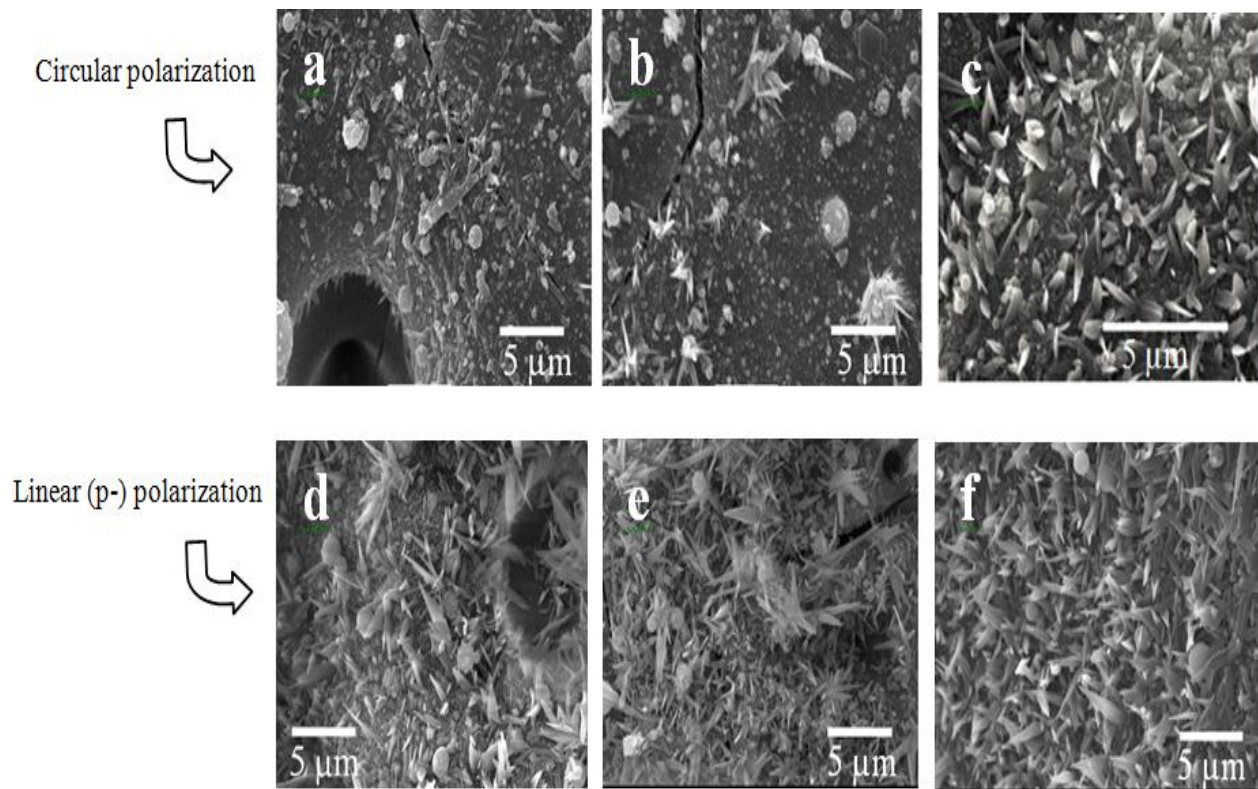


Figure 5-8: SEM images of glass targets irradiated with circularly polarized pulses (a,b,c), and linearly (p-) polarized laser pulses (d,e,f): a),d) 4MHz, 0.25ms; b),e) 4MHz, 0.5ms; c),f) 8MHz, 0.25ms

Looking at Figure 5-8 SEM images these changes can better be understood. Figure 5-8a shows the SEM image of target irradiated with circular polarization laser with 4MHz repetition rate at dwell time of 0.25ms. It can be seen from this image that there is no evident of tips growth most likely because there was not enough material ablated into plasma which could get redeposited to start the formation of tips. When the target was irradiated with linearly (p-) polarized pulses with same the laser parameters as depicted in Figure 5-8d, the high number of nanotips found to be growing on the target surface. This is only possible if the linearly polarized pulses ablated adequate amount of material from target into the plasma in order for the nanotips to initiate and complete the growth. To further make sure if this is the case for other laser parameters with linear polarization, we also irradiated targets at 0.5ms dwell time for 4MHz, and at 0.25ms for

8MHz. The corresponding SEM images of these experiments are shown in Figure 5-8. For each parameter it was found that the growth of nanotips improved in terms of density of nanotips over large target surface at each parameter. From this result, it can be understood that the linear (p-) polarization does not really alter the nanotips growth mechanism but rather it enhances it. Since linearly polarized pulses ablate material more effectively even at the same pulse energy in comparison to circular polarization, it will take very less number of pulses while using linear polarization to reach each growth stage explained in Figure 5-7. Now that we know how the growth of nanotips is effected according to various femtosecond laser parameters, it will be beneficial to perform *in situ* analysis of the plasma expansion, the process temperature and pressure gradient for each combination of the laser parameters. This future work will help us find out the exact combination of femtosecond laser parameters which will produces more uniform and maximum number of nanotips over large surface of the dielectric targets.

Chapter 6: Conclusion and Future Work

6.1 Conclusion

In conclusion, a study of growth mechanism for the leaf-like nanotips on femtosecond laser irradiated transparent dielectric material has been discussed in this thesis report. Conventionally, the nanotips of only the crystalline materials has been produced using various clean room techniques that demand long processing time, complicated equipment, and high vacuum. This thesis proposed a simple, one step technique that requires the irradiation of a glass target using femtosecond laser pulses in presence of background nitrogen gas flow in ambient air. Another advantage of this method is that it does not require catalyst. The target itself acts as the source for the building material and as the substrate upon which these nanotips grow. It was demonstrated that three kinds of nanotips growth is possible on the target surface: randomly oriented multiple tips growing from a single large droplet, individual tip growing from a small droplet, and multiple tips growing from deposited layer of molten material. Unlike previously produced nanotips, the nanotips produced through this method are amorphous.

The growth mechanism is discussed based on the well-established vapour condensation theory. Upon laser irradiation, high energy plasma is generated above the target material. The condensates of the plasma create numerous nanoparticles which deposit on to the surface of the target material. The force imbalance that exists on those deposited nanoparticles is proposed to be the responsible factor for the initiation of the stems. These randomly oriented stems are showered with the continuous rain of plasma condensates resulting in growth of nanotips in direction of stems. The negative thermal expansion between absolute zero and room temperature

of silicate networks in studied glass is also believed to be responsible for the reduction of cross section of nanotips along its length.

The influence of the various laser conditions on nanotips growth has also been investigated. It was found that as the laser pulse width was increased there was a clear transformation from being the individual tips growth from small-to-large sized droplets to multiples nanotips growth from large volumes of deposited molten material. The repetition rate and the dwell time both changes the number of pulses that hit a given spot. As a result, the right combination of the repetition rate and dwell time provides the number of pulses that ablate adequate material into the plasma for the growth of very densely packed nanotips. It was demonstrated for three different repetition rates for a given dwell time. Later the effect of dwell time on the growth of nanotips was discussed for particular repetition rate. There was clear transformation from just the growth of small stems to fully grown nanotips from low dwell time to high dwell time. Finally the influence of laser polarization was discussed. It is known that linearly (p-) polarized laser beams ablate material more efficiently from target in comparison to circularly polarized laser beam. As a result, it would take less number of pulses to ablate adequate material into the plasma to produce densely packed nanotips. This was demonstrated for several laser parameters. This study provides insight into the control of nanotips growth.

6.2 Future work proposal

The Future work should involve the *in situ* analysis of plasma interactions with nitrogen gas flow and incoming laser pulses. The pressure and the temperature gradient of target surface as well as

of the expanding plasma should also be analyzed *in situ*. Understanding the aforementioned phenomena *in situ* will help us grow more uniform nanotips over the target surface. The further study should also be conducted to find out the mechanical, electrical and optical properties of these nanotips.

Appendix

Appendix A: Nanotips generated for circular polarization

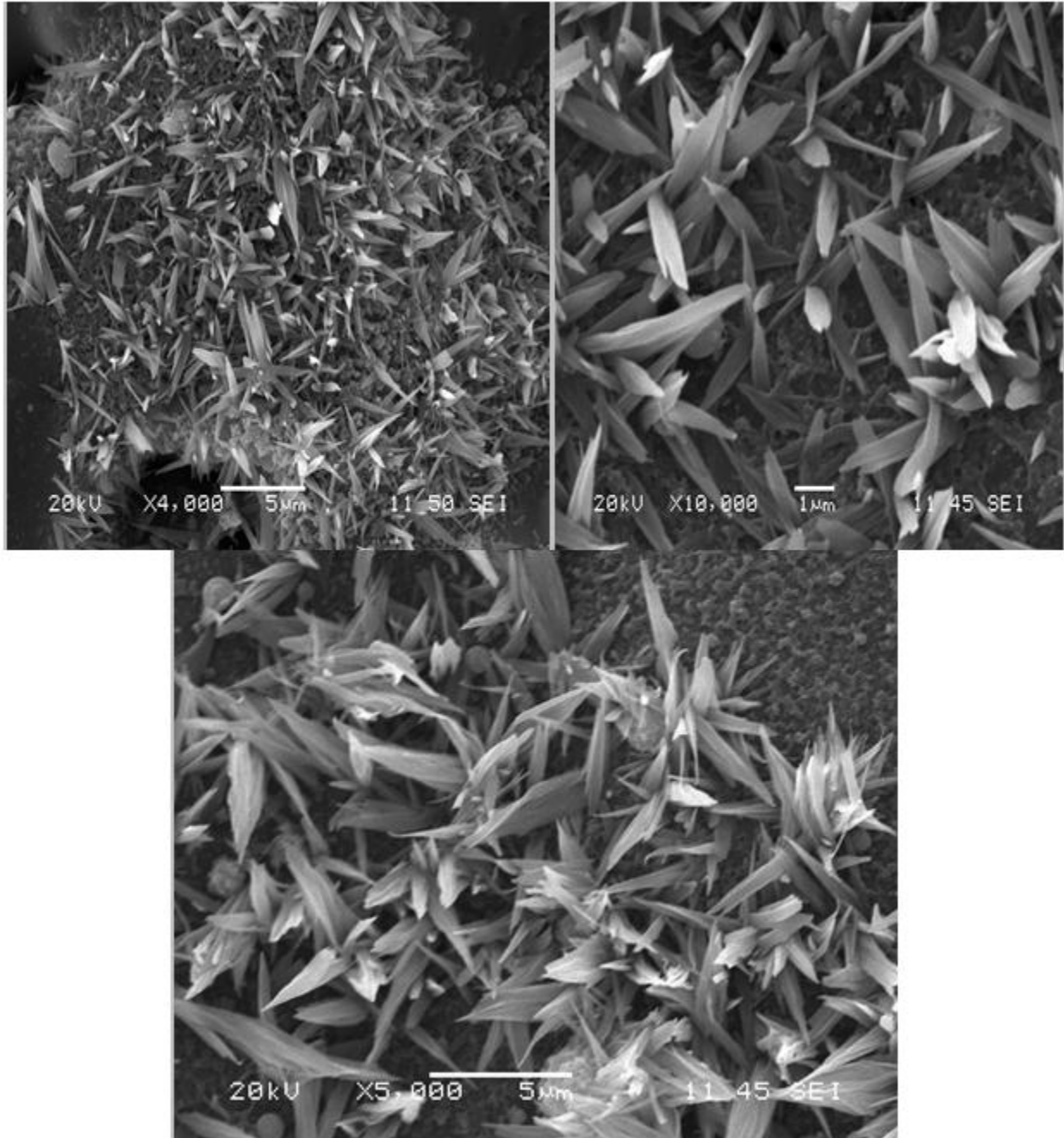


Figure A-1: Nanotips generated at 12MHz repetition rate, various dwell times: Circular Polarization

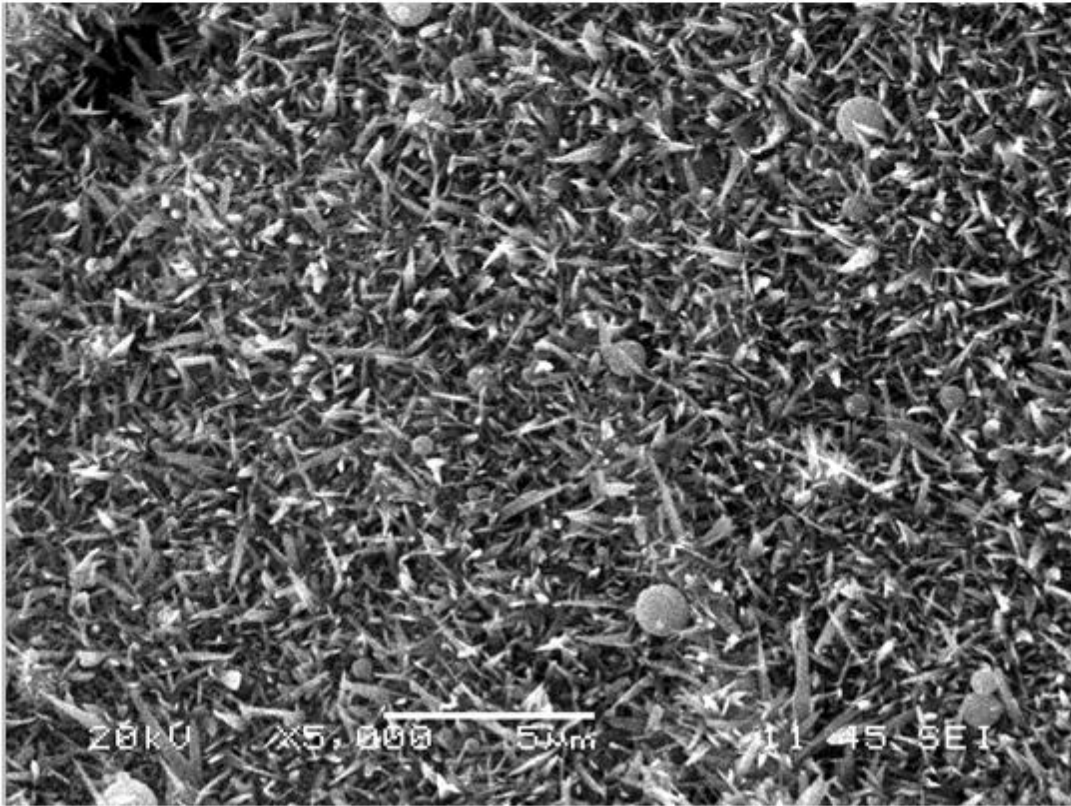
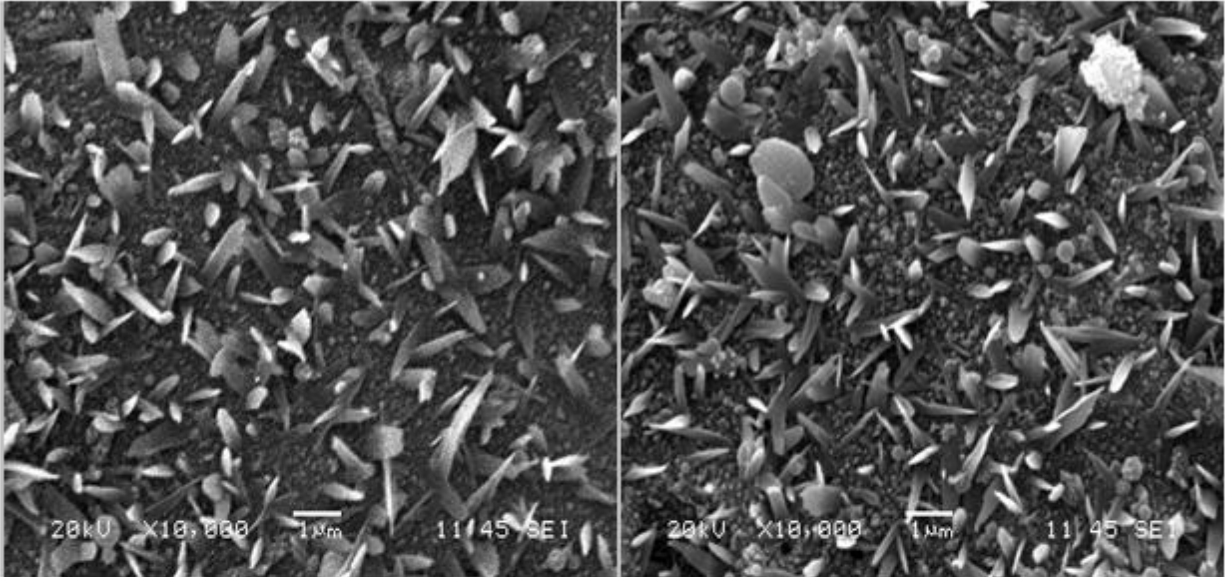


Figure A-2: Nanotips generated at 8MHz repetition rate, various dwell times: Circular Polarization

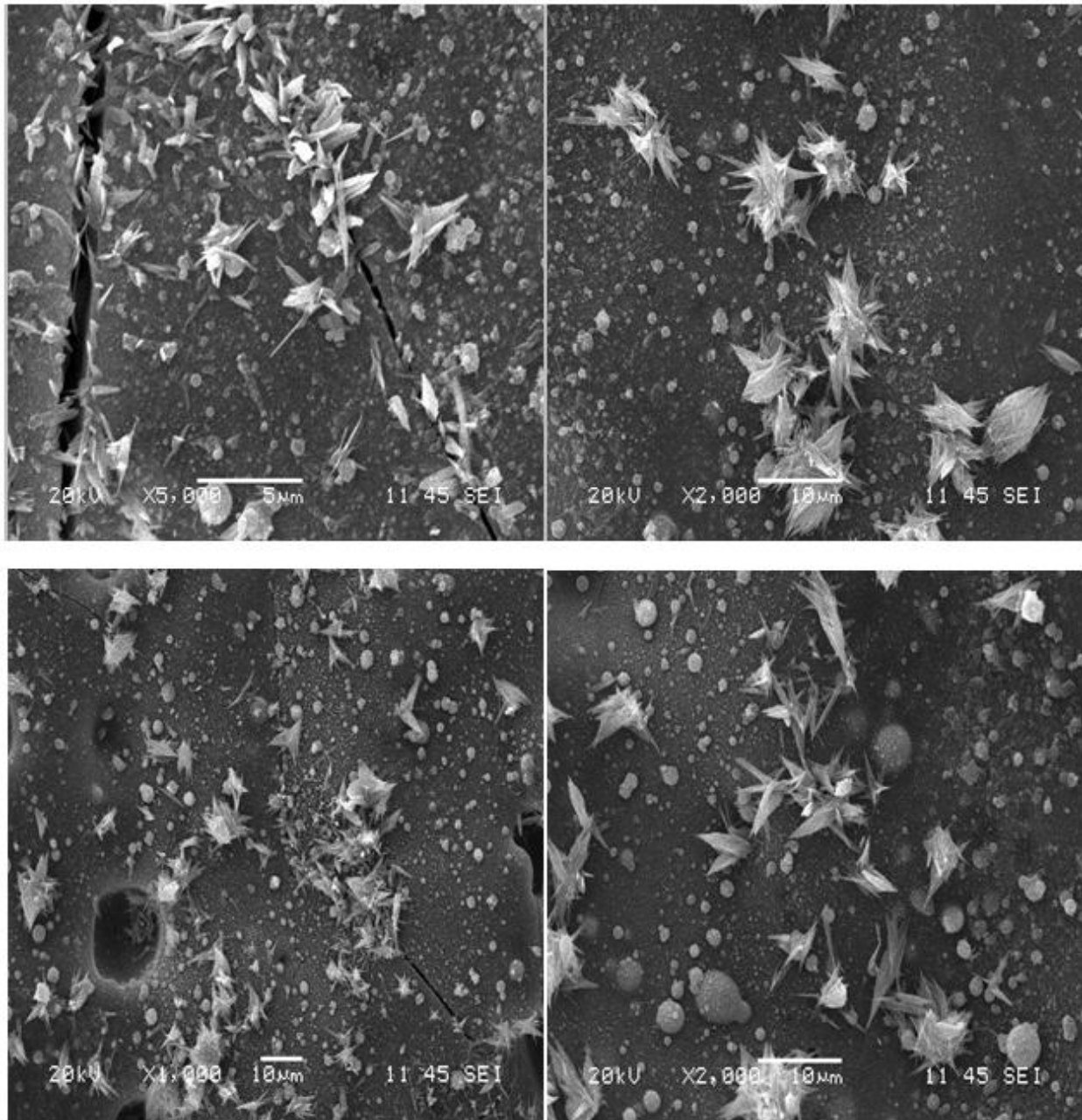


Figure A-3: Nanotips generated at 4MHz repetition rate, various dwell times: Circular Polarization

Appendix B: Nanotips generated for linear polarization

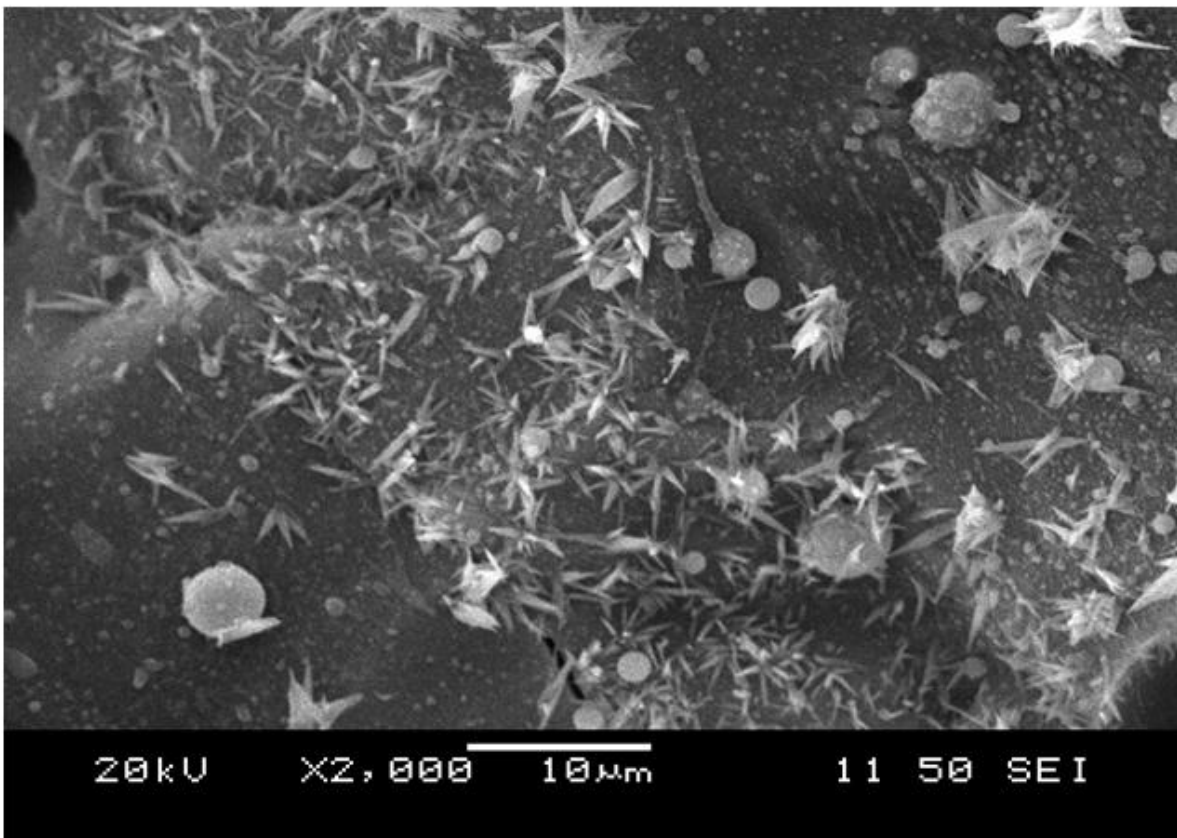
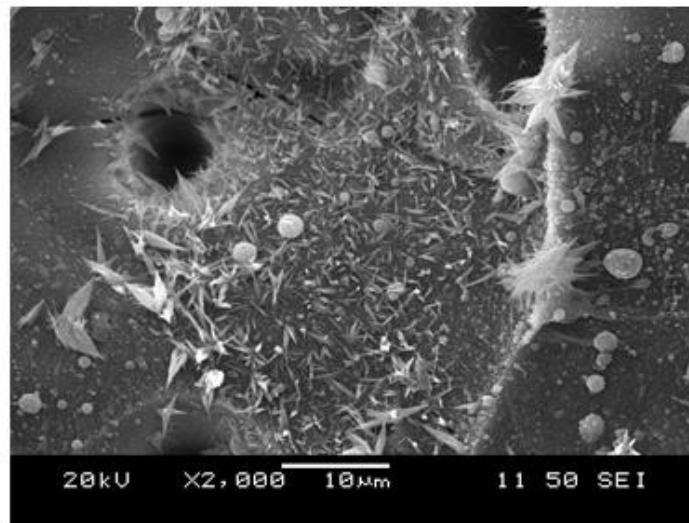


Figure B-1: Nanotips generated at 12MHz repetition rate, various dwell times: Linear (p-) Polarization

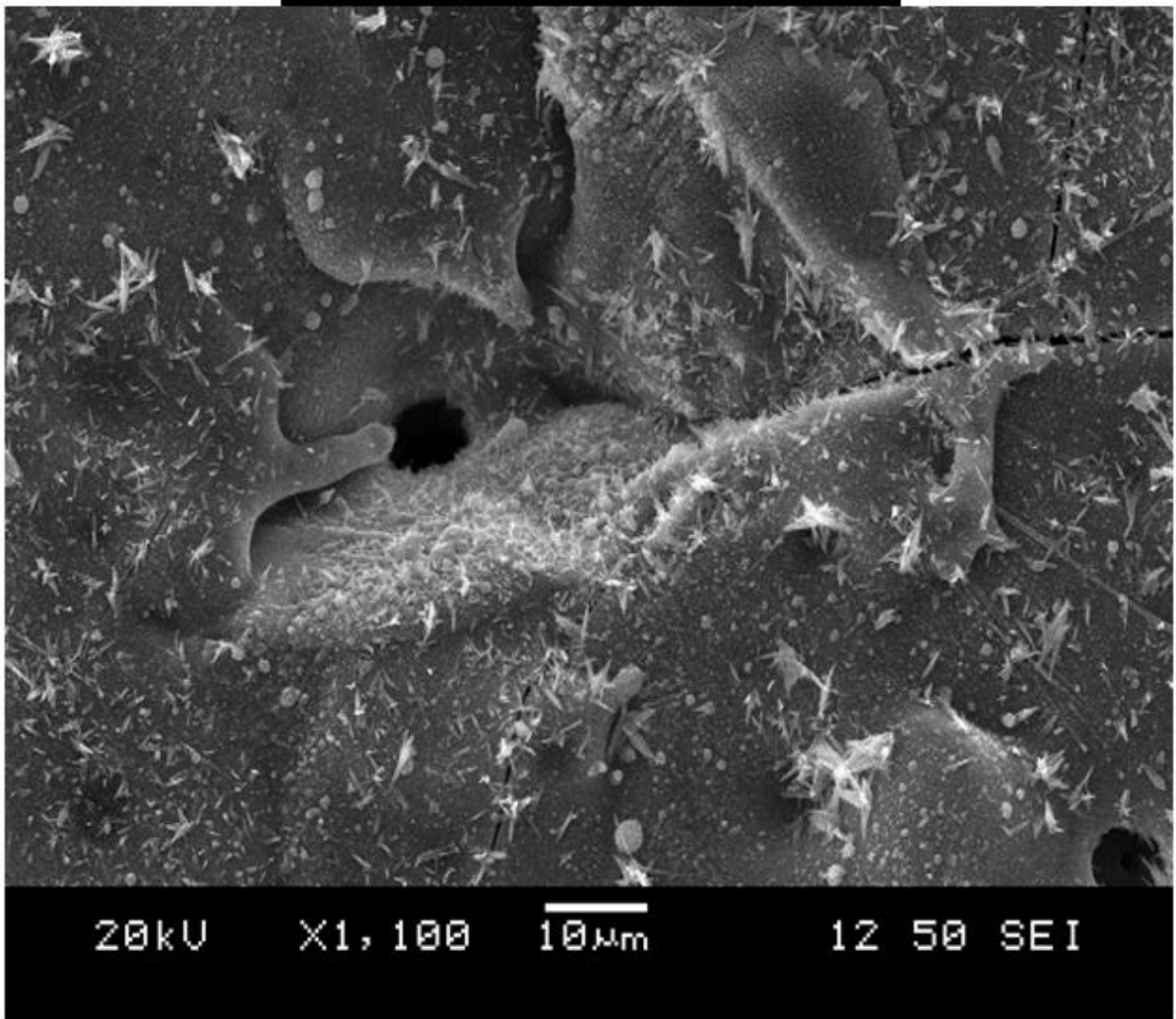
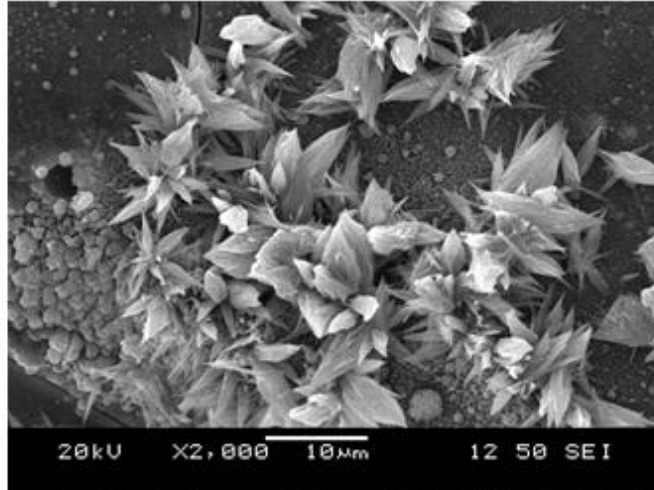


Figure B-2: Nanotips generated at 8MHz repetition rate, various dwell times: Linear (p-) Polarization

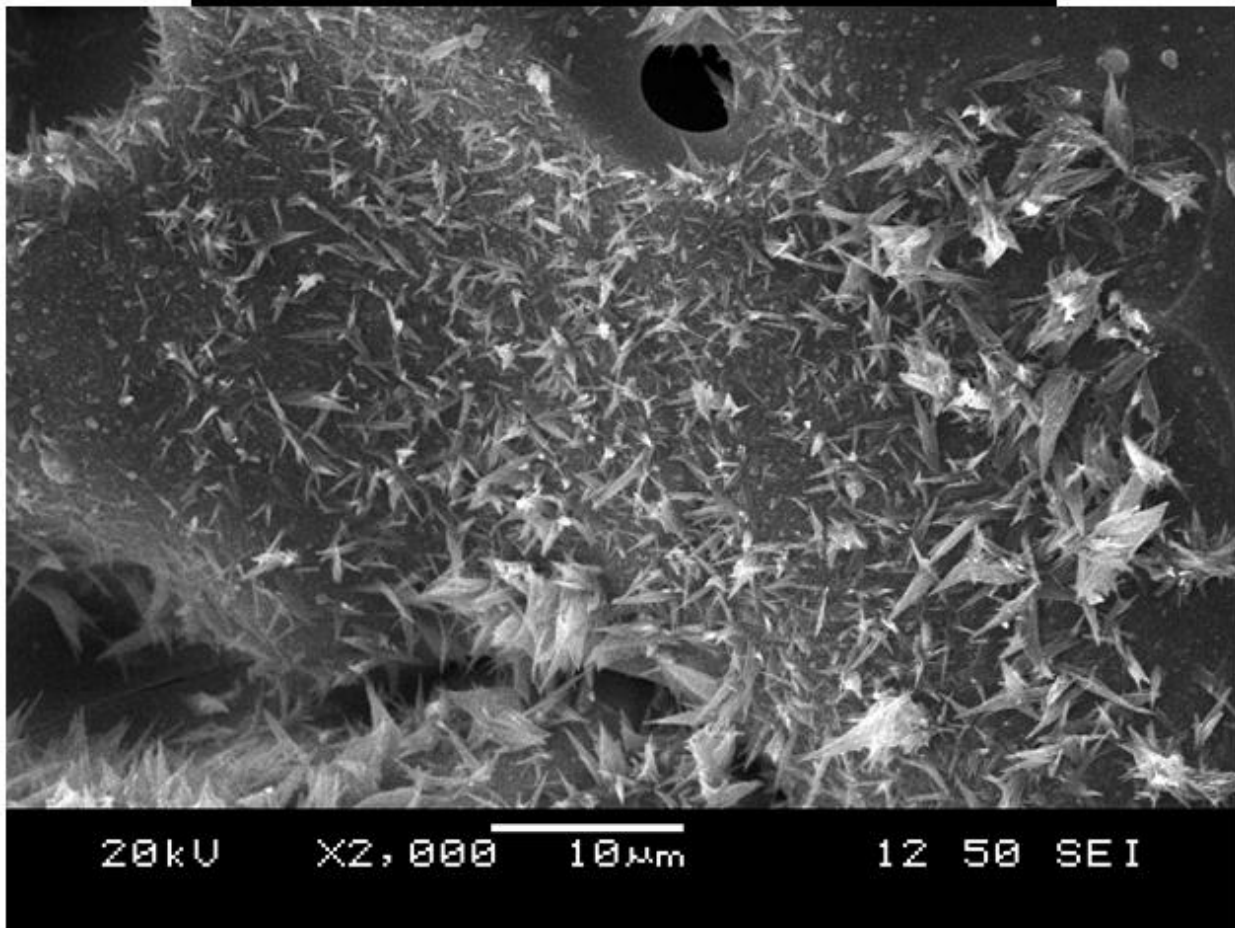
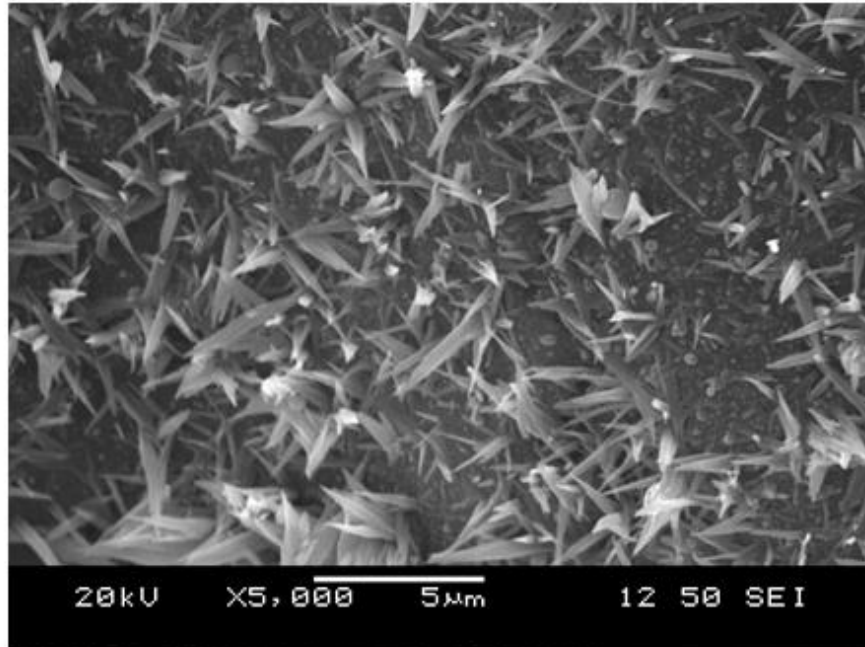


Figure B-3: Nanotips generated at 8MHz repetition rate, various dwell times: Linear (p-) Polarization

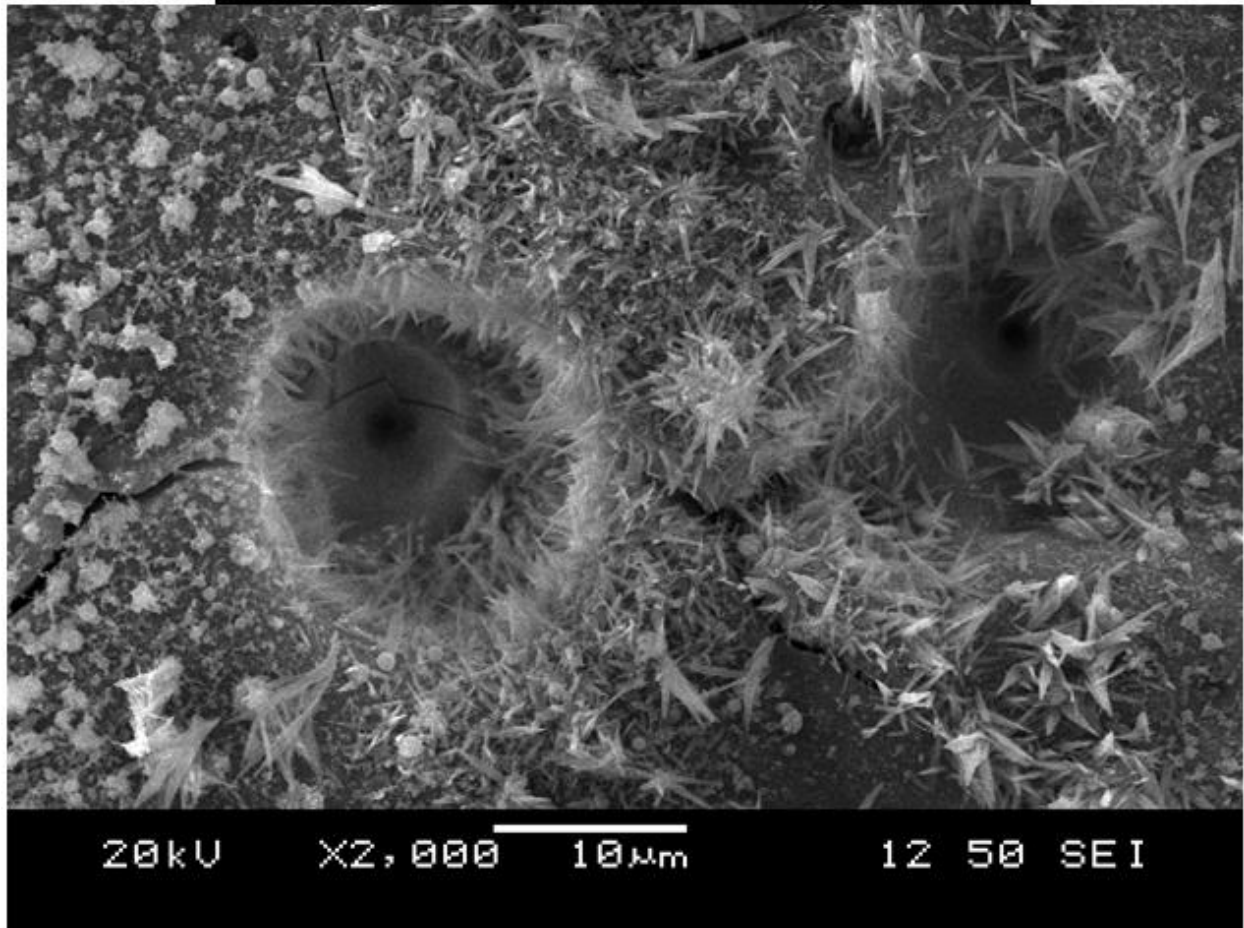
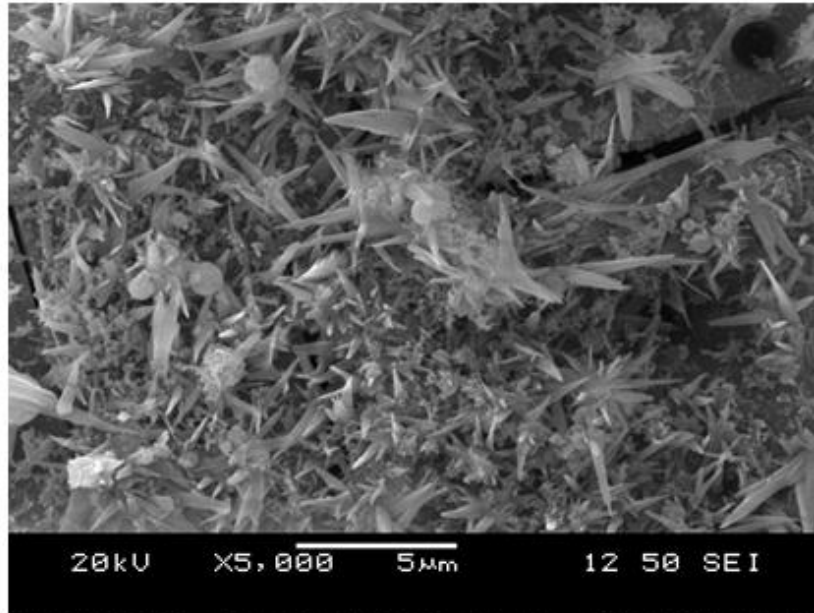


Figure B-4: Nanotips generated at 4MHz repetition rate, various dwell times: Linear (p-) Polarization

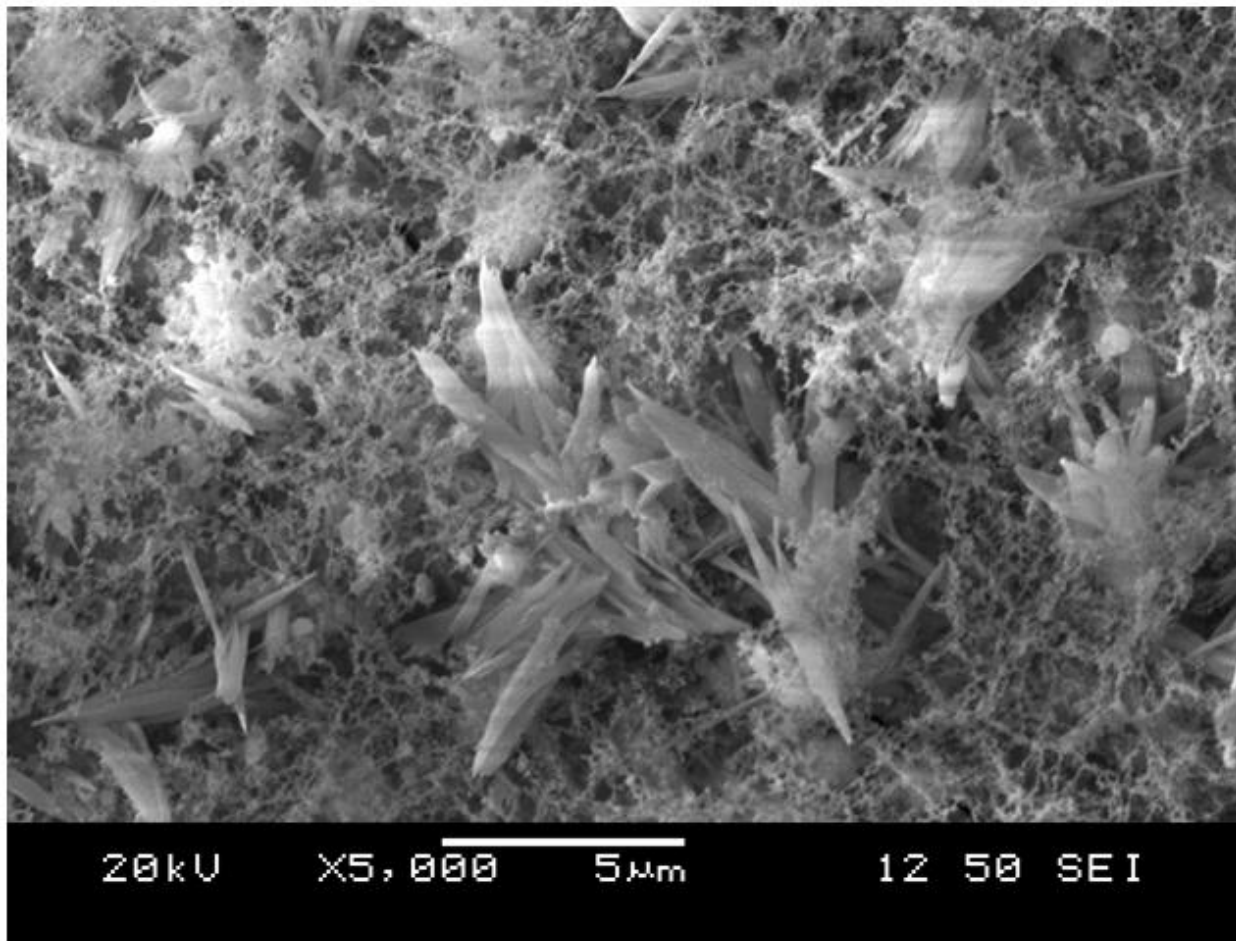
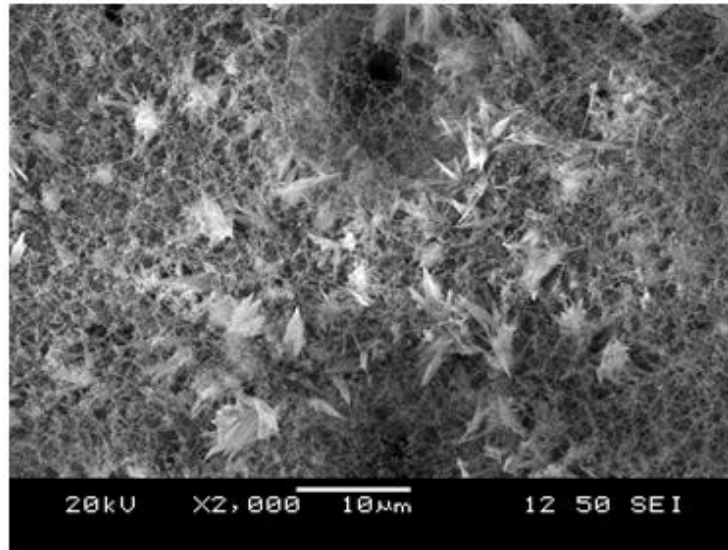


Figure B-5: Nanotips covered with nanofibrous networks

Appendix C: Nanotips generated on window glass

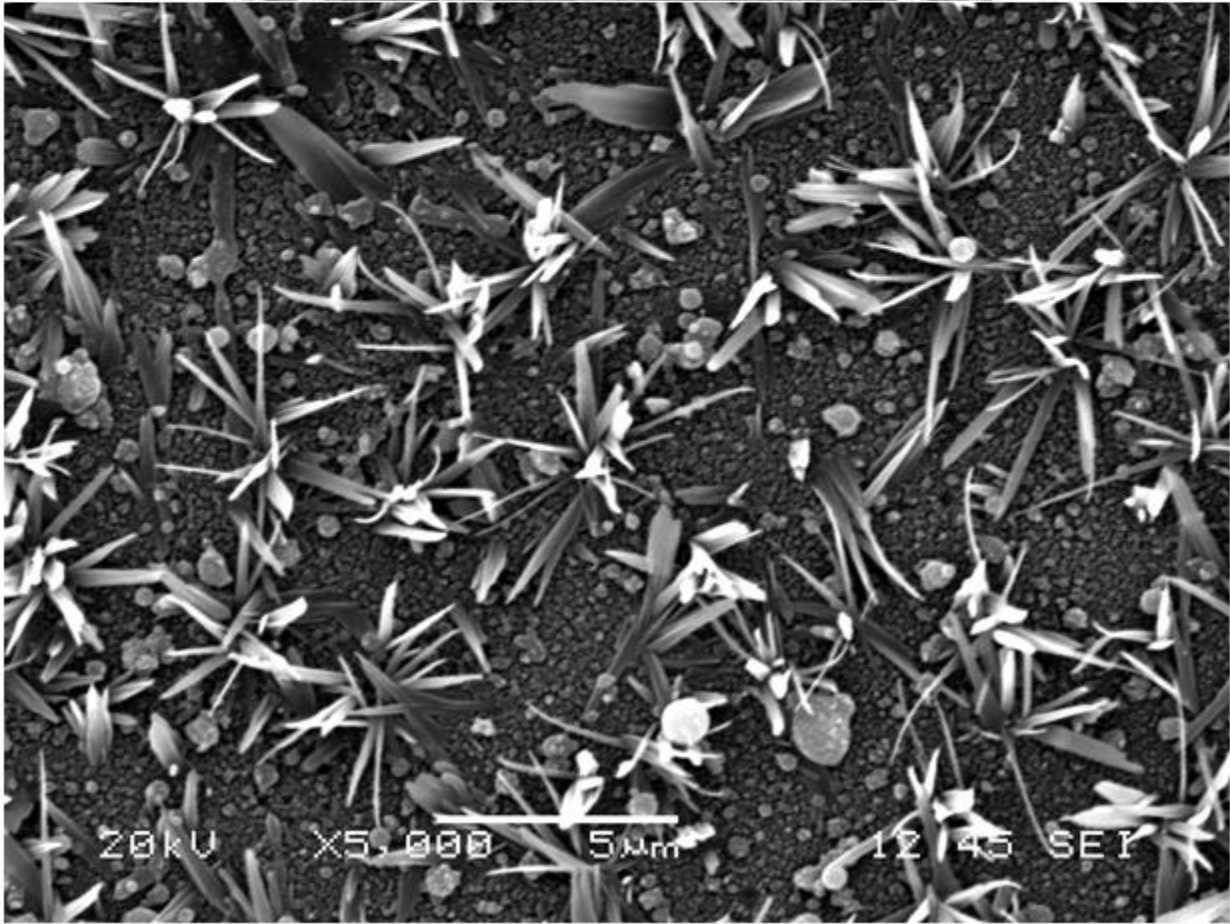
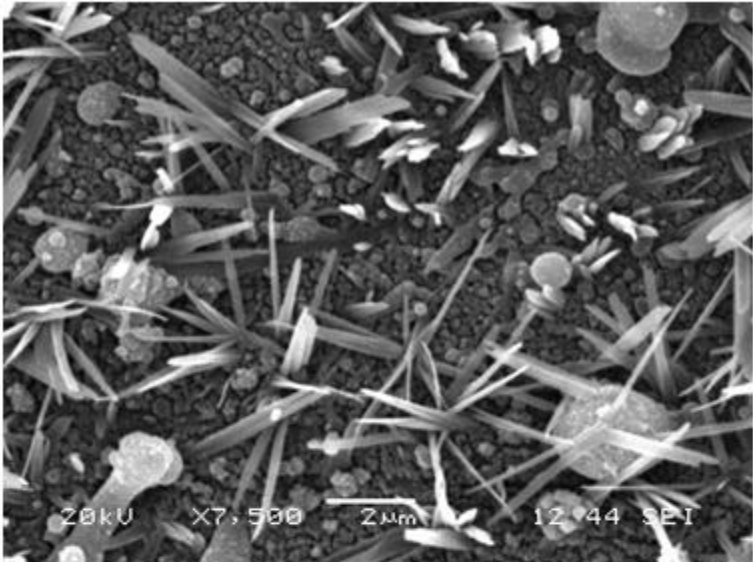


Figure C-1: Nanotips generated on Window Glass

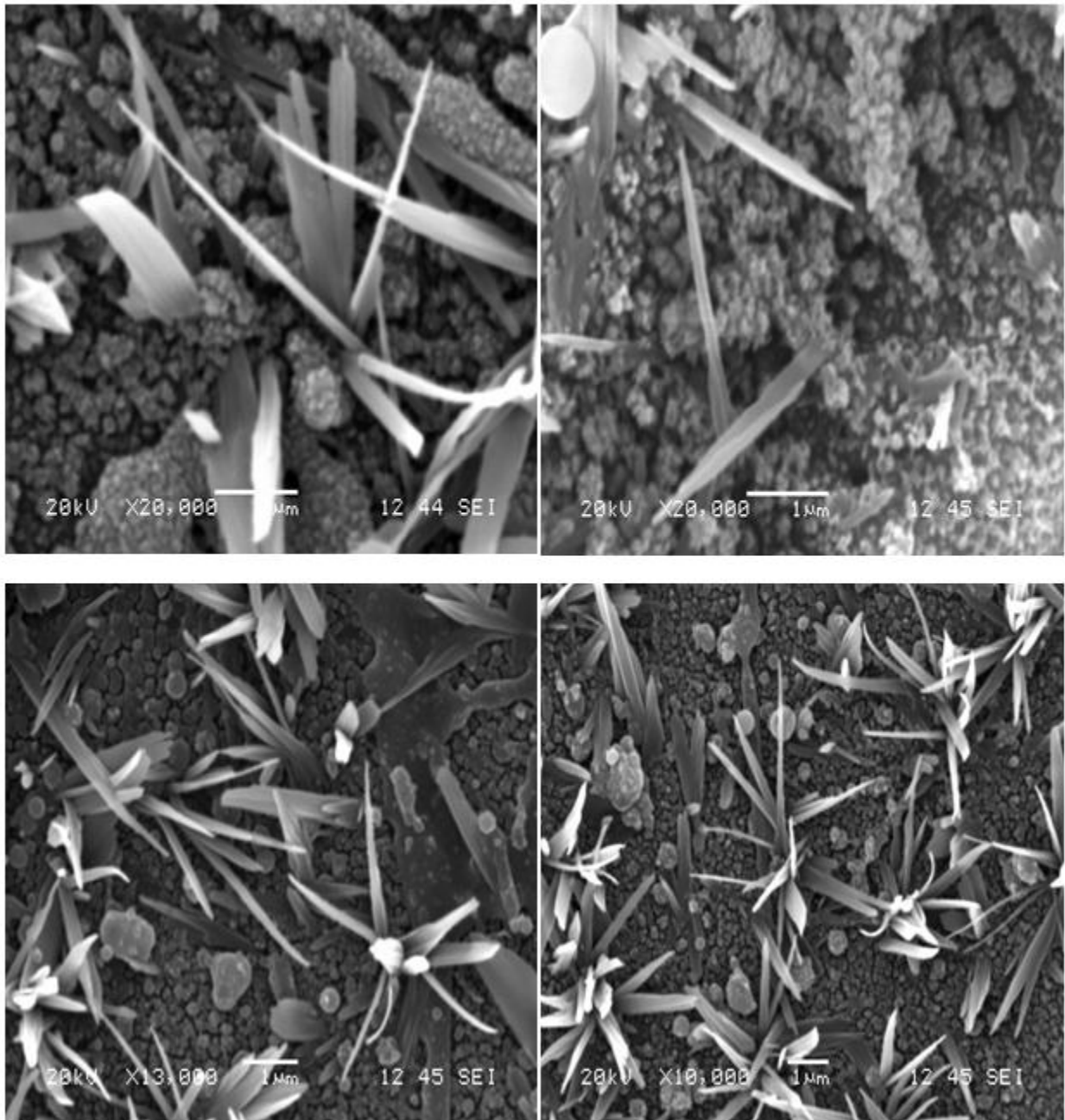


Figure C-2: Nanotips generated on Window Glass

Appendix D: List of Journal Submissions

The following is the list of submitted and in-progress journal articles from the research work of the current thesis:

1. Nikunj B. Patel, Bo Tan, and Krishnan Venkatakrishnan, “The leaf-like nanotips synthesized on femtosecond laser irradiated dielectric material,” *Journal of Nanoparticle Research*, 2011.
2. Nikunj B. Patel, Bo Tan, and Krishnan Venkatakrishnan, “Study of growth of nanostructures with nanoscale apex induced by femtosecond laser at mega-hertz frequency,” (To be submitted September 2011).

References

- [1] M. Sivakumar, K. Venkatakrishnan and B. Tan, "Synthesis of nanoscale tips using femtosecond laser radiation under ambient condition," *Nanoscale Research Letters*, vol. 5, pp. 438-441, 2010.
- [2] S. Chattopadhyay, L. - Chen and K. - Chen, "Nanotips: Growth, model, and applications," *Critical Reviews in Solid State and Materials Sciences*, vol. 31, pp. 15-53, 2006.
- [3] S. J. Chang, C. H. Hsiao, S. B. Wang, Y. C. Cheng, T. C. Li, S. P. Chang, B. R. Huang and S. C. Hung, "A quaternary ZnCdSeTe nanotip photodetector," *Nanoscale Research Letters*, vol. 4, pp. 1540-1546, 2009.
- [4] K. - Chen, C. - Hsu, H. - Lo, S. Chattopadhyay, C. T. Wu, J. - Hwang, D. Das and L. - Chen, "Generally applicable self-masking technique for nanotips array fabrication," *Tamkang Journal of Science and Engineering*, vol. 7, pp. 129-134, 2004.
- [5] C. - Cheng, S. - Chao and Y. - Chen, "Enhancement of field emission in nanotip-decorated ZnO nanobottles," *J. Cryst. Growth*, vol. 311, pp. 4381-4384, 2009.
- [6] C. Liu, Z. Hu, Q. Wu, X. Wang, Y. Chen, H. Sang, J. Zhu, S. Deng and N. Xu, "Vapor-solid growth and characterization of aluminum nitride nanocones," *J. Am. Chem. Soc.*, vol. 127, pp. 1318-1322, 2005.
- [7] B. B. Wang, K. Ostrikov, Z. L. Tsakadze and S. Xu, "Analysis of photoluminescence background of Raman spectra of carbon nanotips grown by plasma-enhanced chemical vapor deposition," *J. Appl. Phys.*, vol. 106, 2009.
- [8] D. F. Farson, H. W. Choi, B. Zimmerman, J. K. Steach, J. J. Chalmers, S. V. Olesik and L. J. Lee, "Femtosecond laser micromachining of dielectric materials for biomedical applications," *J. Micromech Microengineering*, vol. 18, 2008.

- [9] J. Zhong, S. Muthukumar, G. Saraf, H. Chen, Y. Chen and Y. Lu, "ZnO nanotips grown on Si substrates by metal-organic chemical-vapor deposition," *J Electron Mater*, vol. 33, pp. 654-657, 2004.
- [10] S. Muthukumar, H. Sheng, J. Zhong, Z. Zhang, N. W. Emanetoglu and Y. Lu, "Selective MOCVD growth of ZnO nanotips," *IEEE Transactions on Nanotechnology*, vol. 2, pp. 50-54, 2003.
- [11] C. -. Hsu, H. -. Lo, C. -. Chen, C. T. Wu, J. -. Hwang, D. Das, J. Tsai, L. -. Chen and K. -. Chen, "Generally applicable self-masked dry etching technique for nanotip array fabrication," *Nano Letters*, vol. 4, pp. 471-475, 2004.
- [12] G. Shen, Y. Bando, B. Liu, D. Golberg and C. -. Lee, "Characterization and field-emission properties of vertically aligned ZnO nanonails and nanopencils fabricated by a modified thermal-evaporation process," *Advanced Functional Materials*, vol. 16, pp. 410-416, 2006.
- [13] B. C. Stuart, M. D. Feit, S. Herman, A. M. Rubenchik, B. W. Shore and M. D. Perry, "Nanosecond-to-femtosecond laser-induced breakdown in dielectrics," *Physical Review B - Condensed Matter and Materials Physics*, vol. 53, pp. 1749-1761, 1996.
- [14] I. H. Chowdhury, A. Q. Wu, X. Xu and A. M. Weiner, "Ultra-fast laser absorption and ablation dynamics in wide-band-gap dielectrics," *Applied Physics A: Materials Science and Processing*, vol. 81, pp. 1627-1632, 2005.
- [15] L. D'Alessio, R. Teghil, M. Zaccagnino, I. Zaccardo, D. Ferro and V. Marotta, "Pulsed laser ablation and deposition of bioactive glass as coating material for biomedical applications," *Appl. Surf. Sci.*, vol. 138-139, pp. 527-532, 1999.
- [16] S. Amoroso, R. Bruzzese, X. Wang and J. Xia, "Propagation of a femtosecond pulsed laser ablation plume into a background atmosphere," *Appl. Phys. Lett.*, vol. 92, 2008.
- [17] P. Spiga, J. Hermann, T. Itina, D. Grojo, D. Neamtu, D. Pailharey and W. Marine, "Investigation of nanoparticle formation in a plasma produced by femtosecond laser ablation of gold," in *AIP Conference Proceedings*, 2005, pp. 197-200.

- [18] D. B. Geohegan, A. A. Puretzky, G. Duscher and S. J. Pennycook, "Time-resolved imaging of gas phase nanoparticle synthesis by laser ablation," *Appl. Phys. Lett.*, vol. 72, pp. 2987-2989, 1998.
- [19] J. Koch, S. Schlamp, T. Rösger, D. Fliegel and D. Günther, "Visualization of aerosol particles generated by near infrared nano- and femtosecond laser ablation," *Spectrochimica Acta - Part B Atomic Spectroscopy*, vol. 62, pp. 20-29, 2007.
- [20] D. Breitling, S. Klimentov and F. Dausinger, "Interaction with Atmosphere," *Femtosecond Technology for Technical and Medical Applications*, pp. 75-91, 2004.
- [21] E. Pfender, J. Fincke and R. Spores, "Entrainment of cold gas into thermal plasma jets," *Plasma Chem. Plasma Process.*, vol. 11, pp. 529-543, 1991.
- [22] P. M. Ossi and A. Bailini, "Cluster growth in an ablation plume propagating through a buffer gas," *Applied Physics A: Materials Science and Processing*, vol. 93, pp. 645-650, 2008.
- [23] M. S. Tillack, D. W. Blair and S. S. Harilal, "The effect of ionization on cluster formation in laser ablation plumes," *Nanotechnology*, vol. 15, pp. 390-403, 2004.
- [24] E. Pfender, "Plasma jet behavior and modeling associated with the plasma spray process," *Thin Solid Films*, vol. 238, pp. 228-241, 1994.
- [25] R. Spores and E. Pfender, "Flow structure of a turbulent thermal plasma jet," *Surface and Coatings Technology*, vol. 37, pp. 251-270, 1989.
- [26] M. R. Vukcevic, "A new interpretation of the anomalous properties of vitreous silica," *J. Non Cryst. Solids*, vol. 11, pp. 25-63, 1972.
- [27] C. -. Fan and J. P. Longtin, "Modeling optical breakdown in dielectrics during ultrafast laser processing," *Appl. Opt.*, vol. 40, pp. 3124-3131, 2001.

- [28] H. Varel, D. Ashkenasi, A. Rosenfeld, R. Herrmann, F. Noack and E. E. B. Campbell, "Laser-induced damage in SiO₂ and CaF₂ with picosecond and femtosecond laser pulses," *Applied Physics A: Materials Science and Processing*, vol. 62, pp. 293-294, 1996.
- [29] N. Sanner, O. Utéza, B. Bussiere, G. Coustillier, A. Leray, T. Itina and M. Sentis, "Measurement of femtosecond laser-induced damage and ablation thresholds in dielectrics," *Applied Physics A: Materials Science and Processing*, vol. 94, pp. 889-897, 2009.
- [30] D. Du, X. Liu, G. Korn, J. Squier and G. Mourou, "Laser-induced breakdown by impact ionization in SiO₂ with pulse widths from 7 ns to 150 fs," *Appl. Phys. Lett.*, vol. 64, pp. 3071-3073, 1994.
- [31] B. C. Stuart, M. D. Feit, A. M. Rubenchik, B. W. Shore and M. D. Perry, "Laser-induced damage in dielectrics with nanosecond to subpicosecond pulses," *Phys. Rev. Lett.*, vol. 74, pp. 2248-2251, 1995.
- [32] C. B. Schaffer, J. F. García and E. Mazur, "Bulk heating of transparent materials using a high-repetition-rate femtosecond laser," *Applied Physics A: Materials Science and Processing*, vol. 76, pp. 351-354, 2003.
- [33] C. W. Hee, B. K. A. Ngoi, L. E. N. Lim, K. Venkatakrisnan and W. L. Liang, "Effect of polarization on femtosecond pulsed laser ablation of surface relief gratings using a novel interferometer," *Opt. Laser Technol.*, vol. 37, pp. 93-98, 2005.
- [34] S. Camacho-López, R. Evans, L. Escobar-Alarcón, M. A. Camacho-López and M. A. Camacho-López, "Polarization-dependent single-beam laser-induced grating-like effects on titanium films," *Appl. Surf. Sci.*, vol. 255, pp. 3028-3032, 2008.
- [35] K. Venkatakrisnan, B. Tan, P. Stanley and N. R. Sivakumar, "The effect of polarization on ultrashort pulsed laser ablation of thin metal films," *J. Appl. Phys.*, vol. 92, pp. 1604, 2002.